Article

Not peer-reviewed version

Towards Sustainable Food Packaging: Mechanical Recycling Effects on Thermochromic Polymers Performance

Colette Breheny * , Declan Mary Colbert , Gilberto Bezerra , Joseph Geever , Luke M. Geever *

Posted Date: 21 March 2025

doi: 10.20944/preprints202503.1564.v1

Keywords: thermochromic pigments; food packaging; mechanical recycling; sustainability; polymer degradation

 doi:10.20944/preprints202503.1564.v1

Article

Towards Sustainable Food Packaging: Mechanical Recycling Effects on Thermochromic Polymers Performance

Colette Breheny *, Declan Mary Colbert, Gilberto Bezerra, Joseph Geever and Luke M. Geever *

Polymer, Recycling, Industrial, Sustainability and Manufacturing (PRISM) Research Institute, Technological University of the Shannon, University Road, N37 HD68 Athlone, Ireland

* Correspondence: colette.breheny@tus.ie; luke.geever@tus.ie

Abstract: Integrating thermochromic pigments (TP) into food packaging offers significant benefits for monitoring temperature variations, improving food safety, and reducing waste. However, the recyclability of such materials remains underexplored, particularly regarding the retention of their optical and mechanical properties after repeated recycling. Addressing this gap, this research aims to evaluate how mechanical recycling affects key properties of polypropylene (PP) blends containing varying TP concentrations. Three formulations—PP100/TP0 (0% TP), PP98/TP2 (2% TP), and PP92/TP8 (8% TP) were subjected to five recycling cycles, with changes in thermal stability, color transition behavior, mechanical integrity, and surface morphology analyzed. Results indicate that PP100/TP0 maintains its mechanical integrity with minimal degradation across recycling cycles. However, blends containing TP exhibited progressive deterioration, with PP98/TP2 displaying moderate reductions in mechanical strength and thermochromic efficiency, while PP92/TP8 showed significant degradation, including increased activation temperatures and color vibrancy loss. These effects were attributed to polymer breakdown, pigment aggregation, and altered crystallinity. Despite the limitations of recyclability, this study provides critical insights into the feasibility of TP in sustainable intelligent food packaging. Further research is required to enhance TP stability during reprocessing, ensuring long-term functionality in circular packaging systems.

Keywords: thermochromic pigments; food packaging; mechanical recycling; sustainability; polymer degradation

1. Introduction

Material science is an interdisciplinary field that studies materials and their properties. It is a challenging and stimulating area of research characterized by rapid and numerous breakthroughs, including novel materials [1]. Among novel materials, smart polymers are gaining interest because of their capacity to respond to stimuli in their environment in a controlled manner [2]. Smart polymers can exhibit various responses, such as changes in shape, solubility, or optical properties, depending on the applied stimulus [3]. One notable example is smart polymers that undergo color changes in response to external stimuli such as pH (chemochromogenic), light (photochromogenic), temperature (thermochromogenic), and magnetic fields (magnetochromogenic) [4]. Among these, thermochromic polymers (TP) stand out for their distinct ability to alter color in response to changes in temperature [5]. As noted by several studies, TP are attractive to numerous applications, including food packaging [6–8].

Integrating thermochromic pigments (TP) into packaging materials that meet food safety standards offers a promising solution for monitoring recommended food storage conditions throughout the supply chain [9]. Food packaging protects food from environmental elements such as oxygen, moisture, light, temperature, and microorganisms [10]. Through its ability to detect temperature changes, TP packaging thereby aids in maintaining food quality and prolonging the

 doi:10.20944/preprints202503.1564.v1

shelf life of the food [11]. Customer awareness surrounding food safety and the desire to reduce food waste has created a demand for intelligent food packaging [12]. By incorporating TP into food packaging, food suppliers can reduce the likelihood of spoiled food by providing customers with vital information regarding the supply chain storage temperature of the packaged food [13].

TP undergo a reversible phase transition at a specific temperature [14,15]. This physical change alters the material's optical characteristics, resulting in a color change [16]. The color modification is intended at specific temperatures, such as room temperature (22 °C), refrigeration temperature (4 °C), or freezing temperature (-18 °C), indicating whether food items have been subjected to temperatures outside the permitted range [17–19] . Monitoring temperature fluctuations through a visual alteration of the food packaging is particularly important for perishable items, including dairy products, meats, and frozen meals, where even a short exposure to temperatures outside the recommended range can result in food decomposition [20].

While TP offer benefits in food packaging, significant concerns arise from their environmental impact [21]. The extensive use of synthetic polymers, including thermochromic materials, has prompted environmental concerns, mainly surrounding plastic waste [22]. Plastic is one of the most extensively utilized materials in the modern world [23]. The global use of plastic materials is rising due to their durability, cost-efficiency, and lightweight properties [24]. Plastic packaging (i.e., film wraps, bags, and other packaging materials) is the primary form of plastic waste worldwide. In Europe, 39.9% of plastic is utilized for packaging [25], and single-use plastics significantly contribute to plastic pollution [26]. Disposable plastic packaging has increased due to its preservation capabilities, protective qualities, and cost-effectiveness [27].

Food packaging is expanding due to the rising global need for food driven by population increase [28]. Most food packaging is designed for on-the-go consumption and comprises of plastics discarded shortly after use [29]. Plastic environmental contamination, predominantly in coastal and marine ecosystems, is recognized as a severe anthropogenic issue [30]. Microplastics, derived from the decomposition of larger plastic items, have been detected in the food chain, oceans, and rivers, endangering humans and animals [31].

In response to these environmental concerns, there is an increasing demand for recyclable, sustainable packaging materials, thereby contributing to protecting the environment [32]. Fewer than 10% of plastics produced globally are recycled; the remainder is incinerated, deposited in landfills, or released into the environment [33]. Recycling is reusing or transforming waste materials to be reused in producing new products [34]. Four main types of recycling processes exist: primary recycling (closed-loop recycling), secondary recycling (mechanical recycling), tertiary recycling (chemical recycling), and quaternary recycling (energy recovery) [35].

Mechanical recycling is a typical technique for recycling single-use plastics [36]. It involves collecting, sorting, cleaning, and reprocessing plastic waste into new products [37]. It is commonly defined as fragmenting plastics into smaller particles through shredding and shearing, then melting and blending to create a homogeneous polymer mixture [38]. Mechanical recycling mitigates plastic waste and conserves resources by reusing plastic waste that otherwise would be discarded in landfills or the natural environment [39]**.** However, it is challenging to recycle high-performance, multiple-functional plastics [40]. Recycling may substantially alter the properties of the recycled materials, particularly when subjected to multiple recycling cycles. These changes include reduced mechanical strength, thermal stability, and optical characteristics [41].

Numerous studies have examined the impact of mechanical recycling on polymer resins, such as polypropylene [42–44]. However, the effect of mechanical recycling on polymer resins infused with TP, particularly those used in food packaging, is under-researched. This under-exploited area presents a significant gap in understanding the recycling of TP. If temperature sensitivity is compromised, it may become impossible to properly alert customers to temperature changes in food storage [45]. If TP are no longer capable of accurately detecting a discrete temperature change, its distinctive ability to detect and respond optically to temperature fluctuations becomes redundant, making it unsuitable for its intended use in food packaging [46].

 doi:10.20944/preprints202503.1564.v1

The primary concern surrounding the mechanical recycling of TP is the potential degradation of their optical properties [47]. Thermochromic materials exhibit color-changing characteristics due to intricate interactions between the polymer matrix and the thermochromic agent. However, this unique thermochromic property is vulnerable during the recycling process due to additional high processing temperatures and mechanical shear stresses, potentially resulting in the degradation of the thermochromic masterbatch or the formation of defects in the base polymer matrix [48].

In addition to optical properties, smart polymers' mechanical properties are also critical [49]. Food packaging must maintain specific mechanical characteristics to protect food from physical damage during storage, transportation, and distribution [50]. Mechanical properties, such as tensile strength, elongation at break, Young's modulus, and impact resistance, indicate a material's performance [51]. The recycling process can reduce these properties due to the degradation of the polymer chains caused by high processing temperatures [52]. In addition, the presence of thermochromic additives blended with the base polymer could alter the crystallinity of the polymer matrix during recycling, further affecting the material's properties [53].

It remains unknown whether recycling affects the optical and mechanical properties of TP. Understanding the impact of recycling on the properties of TP is central to determining the feasibility of employing TP in food packaging applications. It could inform the development of modifications required to mitigate any potential adverse effects of recycling. To the best of our knowledge, no study has investigated this. This study addresses these research gaps by examining the impact of mechanical recycling on thermochromic food-grade polymers' optical and mechanical properties. Color stability, tensile strength, impact resistance, and other relevant properties will be evaluated through multiple recycling steps. The findings of this study will provide a comprehensive understanding of how recycling affects TP and will offer guidance for recyclable intelligent food packaging materials.

2. Materials and Methods

2.1. Materials

A commercially available food-grade nucleated polypropylene (PP) (Moplen HP548R, Mw 26,000 g/mol, LyondellBasell, UK) was supplied by Ross Polymer (Athlone, Ireland). The material had a density of 0.9 g/cm^3. Additionally, the manufacturer certified the material as suitable for food contact applications.

Thermochromic pigment (ThermoBatch™) obtained from SpotSee®/LCR Hallcrest Ltd. (Chester, UK) was supplied in pellet form with a reversible temperature transition of 41 °C. It had a density of 0.508 g/cm^3 and an MFI range from 15-40 g/10 min.

Unless otherwise stated, all testing was conducted at 23 °C ± 2 °C, in accordance with the requirements of ISO 527-2:2012 [55], ISO 179-1:2023 [54], and other applicable standards. These conditions ensured consistent and reproducible results across tensile, impact, and other property evaluations.

2.2. Preparation of Polypropylene and Thermochromic Pigment Mixture

Binary mixtures of PP as the matrix and TP as the additive were manually dry-mixed by tumbling in a sealed polyethylene bag for five minutes to ensure homogeneity. Each blend weighed 2.5 kg. The components were accurately weighed using a Sartorius LA230P analytical balance (Sartorius, Dublin, Ireland) with a precision of ±0.0001 g. The colored concentrate ThermoBatch™ contained a compatible PP polymeric carrier miscible with the PP matrix. After blending, the samples were conditioned at 23 °C for 24 hours before testing to ensure consistent results. The blend compositions are shown in Table 1.

 doi:10.20944/preprints202503.1564.v1

Table 1. Blend compositions prepared for this study.

Specimen ID.	PP (wt. %)	TP (wt. %)
PP100/TP0	100	0
PP98/TP2	98	2
PP92/TP8	92	8

2.3. Injection Molding

Injection molding is a processing technology that melts polymer material with the aid of a screw and external heating bands and then injects it into a mold to form the equivalent product as the mold cools [56]. Injection molding was carried out per ISO 294-1: 2017 [57]. The blends in Table 1 were processed using an Arburg Allrounder 370E 600 E drive injection molding machine (Arburg, Lossburg, Germany). The machine was fitted with a "two by two" family mold with a double-T runner to produce two tensile (type B1) and two impact (type A1) test specimens. The Arburg machine had a maximum clamping force of 600 kN, a screw diameter of 30 mm, and a maximum calculated stroke volume of 85 cm^3.

The temperature distribution along the barrel was regulated by four temperature controllers, with an additional fifth controller dedicated to managing the nozzle temperature. The temperature profile began at 170 °C at the hopper and progressively increased to 210 °C at the nozzle. A cooling period of 30 s was applied, with an injection pressure of 500 bar, an injection speed of 75 mm/s, and a holding pressure of 300 bar. The mold was maintained at a constant 30 °C using a Piovan Technologies THM 120/EN temperature control unit (JL Goor, Wicklow, Ireland). The mold had a shot size of 50 g. Tensile test specimens (ISO 527-2: 2012 specimen type 1BA [55]) were molded for each blend formulation in Table 1. Charpy impact test specimens (ISO 179-1 2023: specimen type 1, direction of blow edgewise [54]) were produced and notched with a Type A V-notch where required.

2.4. Simulation of Mechanical Recycling.

Mechanical recycling refers to operations that recover plastic solid waste via mechanical processes; thereby, the new recycled material can be converted into new plastic products, substituting for virgin polymers or a portion of virgin polymers [58]. The mechanical recycling process was simulated using a Rapid 150-21 series rotary granulator (Rapid Granulator, Bredaryd, Sweden). The granulation process yielded granules within a 3 mm to 10 mm controlled size range. After granulation, a portion of the material was reserved for subsequent characterization. The remaining granulated material underwent reprocessing through an additional injection molding cycle, followed by another granulation stage. The process of molding and granulation was repeated five times to simulate the degradation effects of repeated mechanical recycling on the polymer material. Specimens for testing were prepared after each recycling cycle, corresponding to 0x, 1x, 2x, 3x, 4x, and 5x reprocessing cycles.

2.5. Visual and Physical Properties

The physical appearance of granulated polymer blends and injection-molded test specimens was assessed to evaluate changes in visual characteristics across mechanical recycling cycles. High-resolution digital photographs of each sample were captured using a high-resolution DSLR camera (Canon EOS 90D) with controlled LED lighting (CRI > 90) to ensure accurate color reproduction. Samples were placed on a neutral, matte white background to enhance contrast. The camera was positioned at a fixed distance and angle relative to the samples to maintain image comparability. Observations focused on parameters such as color uniformity, surface texture, and visible defects (e.g., cracks, streaking, or warping).

MATLAB (version R2024a) software quantified changes in hue, saturation, and brightness (HSB) for the samples by converting Red, Green, and Blue (RGB) values using the rgb2hsv function, ensuring color vibrancy and uniformity tracking. These quantitative assessments complemented

 doi:10.20944/preprints202503.1564.v1

visual observations, providing valuable insight into the effects of mechanical recycling on the visual and aesthetic properties of the materials.

2.6. Color Measurement

The chromatic characteristics and color stability of mechanically multiple recycled thermochromic materials were examined using a portable, handheld sphere spectrophotometer (X-Rite SP62, Grand Rapids, Michigan, USA). Spectrophotometry is a technique used to measure how much light a specimen absorbs or transmits at different wavelengths [59]. The spectrophotometer was calibrated with a white tile and a zero tile in sequence before taking the measurements following the SP60 Series Spectrophotometer user instructions. The color results were presented using the Commission International de l'Eclairage (CIE) chromaticity coordinate system (L*, a*, b*) [60]. In this system, the L* value represents the luminance between black and white and ranges from 0 (black) to 100 (white). The a* and b* parameters represent chromaticity without specific numerical limits. Negative a* values correspond to green, while positive a* values correspond to red. Similarly, negative b* values correspond to blue, and positive b* values to yellow [61]. The differences (ΔL*, Δa*, and Δb*) indicate the variation between the sample and standard in L*, a*, and b* values. In addition, the total color difference (ΔE* ab) was calculated using Equation (1).

$$\Delta E^*_{ab} = [(\triangle L*)^2 + (\triangle a*)^2 + (\triangle b*)^2]^{1/2} \quad (1)$$

where

ΔE^*_{ab} is the color difference between two colors;
$\Delta L*$ is the difference in lightness between the two colors;
$\Delta a*$ is the difference in the red-green axis;
$\Delta b*$ is the difference in the yellow-blue axis.

The color coordinates L^*, a^*, and b^* were recorded according to ISO/CIE 11664-4: 2019 [62] using Oncolor™ (v.6.3.4.4 QC-Lite) software. Five replicates were obtained for each group of samples, and the corresponding means and standard deviations were calculated. This coordinate made it possible to determine the color difference associated with the test specimens. The distance metric, ΔE^*_{ab}, was obtained by following Equation (1), compared with the color coordinates of the initially recycled virgin food grade material, and used as a reference.

2.7. Mass Measurement

Mass measurement before testing polymer samples indicates consistency and comparability in mechanical properties across tests [63]. To ensure the comparability in mechanical properties across different recycling cycles, the mass of tensile test specimens was measured using a Mettler TG50 Thermobalance (Mettler-Toledo, Ohio, USA), with a precision of ±0.0001mg before testing. Five replicate specimens were tested for each recycling cycle to provide statistically robust results. Mass measurements' mean and standard deviation were calculated for each sample set. This approach identified potential trends in mass changes due to material degradation or other factors during the recycling process [64].

2.8. Melt Mass-Flow Rate (MFR) and Melt Volume-Flow rate (MVR) Testing

The melt mass-flow rate (MFR) test measures the mass of polymer, in grams, flowing in 10 minutes (g/10 min) through a heated cylinder and a standard capillary under a prescribed load and temperature [65]. Testing was carried out according to ISO 1133-1: 2022 [66]. A Rosand Precision Advanced Melt Flow Rate System instrument (Labquip, Dublin, Ireland) was used, equipped with an orifice die (2.095 mm diameter, 8 mm capillary length).

Approximately 4 g of polymer pellets were weighed on an Ohaus PA512 Pioneer precision balance (Merck Life Science Limited, Wicklow, Ireland) (±0.01 g accuracy). Testing was carried out at

 doi:10.20944/preprints202503.1564.v1

230 °C using a load of 2.16 kg, as specified in the matrix material data sheet. When the set temperature of the melt flow rate system stabilized for a minimum of 15 minutes, the material was introduced into the barrel using a funnel to aid in the filling. A packing rod compacted the polymer pellets into the barrel, thereby reducing space between pellets, eliminating air gaps, and ensuring the polymer was uniformly melted. The piston was inserted into the barrel, and the preheat timer was activated, counting the 300 s to ensure uniform melting of the polymer sample. Towards the end of the preheat, a 2.16 kg weight was placed on the piston. A piston/weight support held the piston and weights above the upper reference mark before commencing the testing. This support was removed after the preheat was completed. The piston/weight exerted pressure on the polymer, extruding it through the die. The extrudate mass was recorded.

The melt mass-flow rate (MFR), expressed in grams per 10 min, was calculated using Equation 2.

$$MFR\ (T\ , m_{nom}) = \frac{600Xm}{t} \quad (2)$$

where

T is the test temperature, in degrees Celsius;

m_{nom} is the mass, in kilograms, exerting the nominal load;

600 is the factor used to convert grams per second into grams per 10 min (600 s); m is the average mass of the cut-offs, in grams;

t is the cut-off time interval, in seconds.

The melt mass-flow rate (MFR) test measures the mass of the polymer, in grams, flowing in 10 minutes (g/10 min) through a standard capillary under a prescribed load and temperature. Testing was carried out according to ISO 1133-1: 2022 [66].

The melt volume-flow rate (MVR) was calculated from the MFR using Equation (3).

$$MVR\ (T, m_{nom}) = \frac{MFR\ (T, m_{nom})}{\rho} \quad (3)$$

where

ρ is the density of the melt, in grams per cubic centimeter, and is given by the material specification standard or, if not specified therein, obtained at the test temperature.

The MVR test measures the volume of the polymer, in cubic centimeters (cm^3), that flows in 10 minutes (cm^3/10 min) through a standard capillary under a prescribed load and temperature. Testing was conducted in accordance with ISO 1133-1: 2022 [66].

Each sample was tested in quintuplicate, and the mean, standard deviation (SD), and coefficient of variation (CV) for MFR and MVR were calculated to assess consistency. Post-testing, all apparatus components, including the cylinder, piston, and die, were thoroughly cleaned before repeating the testing to prevent contamination. A go/no-go gauge verified the cleanliness of the die.

2.9. Thermal Analysis via Differential Scanning Calorimetry

Differential scanning calorimetry (DSC) is a thermoanalytical method used to measure heat flow (change in enthalpy) as a polymer undergoes controlled temperature fluctuations that induce phase transitions [67]. Key thermal properties, including melting point (T_m) in °C, crystallization temperature (T_{cc}) in °C, enthalpy of melting (ΔH_m) in J/g, and glass transition temperature (T_g) in °C were analyzed using DSC as per ISO 11357-3: 2023 [68].

Thermal characterization was performed on three replicates per sample under a nitrogen atmosphere using a Netzsch Differential Scanning Calorimeter (DSC) 214 Polyma (Netzsch, Wolverhampton, UK), calibrated with indium as the reference material. Samples weighing between 8 mg and 10 mg were precisely measured on a Kern ABJ-NM/ABS-N analytical balance (Kern, Balingen, Germany) (±0.0001 g precision). The polymers were cut into small pieces to ensure uniform thermal distribution and evenly distributed to ensure optimal contact between the sample and the

 doi:10.20944/preprints202503.1564.v1

aluminum crucibles, which were hermetically sealed using a crimping press. An empty pan with a lid served as an inert reference.

DSC scans were conducted at a heating rate of 10 °C/min, covering a temperature range of 20 °C to 230 °C for the test specimens, which had undergone 0, 1, 2, 3, 4, and 5 recycling steps. A constant nitrogen gas flow rate of 40 mL/min was applied to purge volatiles from the sample chamber. DSC measurements were analyzed to determine the transition temperatures using Netzsch Proteus Analysis Manager Software, version 8.0.0.

The percentage of crystallinity (Xc) of the various blended samples was determined using Equation (4) [68].

$$\chi_C = \frac{\Delta H_f}{\Delta H^*_f} \, x \, 100 \tag{4}$$

where

X_c is the relative percentage of crystallinity;

ΔH_f is the melting enthalpy of fusion of the specimen, in joules per gram (J /g);

ΔH^*_f is the melting enthalpy of fusion of 100% crystalline PP, 207 J /g [69].

2.10. Tensile Testing

Tensile testing of polymers is used to evaluate a polymer's mechanical properties by applying a controlled tensile (pulling) force until the sample breaks [70]. Tensile testing was performed on tensile specimens (specimen type 1BA) per ISO 527-2: 2012 [55] to evaluate the mechanical properties of the polymer blends across multiple recycling cycles. The analysis measured **Young's modulus, maximum tensile stress, and tensile strain at break** to assess structural integrity and durability. Each polymer blend, PP100/TP0, PP98/TP2, and PP92/TP8, was tested across five recycling steps (0, 1, 2, 3, 4, and 5 cycles), with five replicate specimens per cycle to ensure statistical robustness.

Tensile test analysis was conducted using an Instron 3400 tensile tester machine (Instron, Norwood, MA, United States), equipped with a 4 kN load cell and Bluehill® software version 4.29 for data acquisition. Each sample was evaluated using five specimens, each with a length of 170 mm, a width of 10 ± 0.04 mm, and a thickness of 4 ± 0.4 mm. A grip gap of 25.4 mm was maintained to ensure uniform clamping. The tensile testing was conducted under quasi-static circumstances at a 10 mm/min strain rate.

2.11. Charpy Impact Testing

The Charpy test is a standardized procedure for evaluating a material's toughness or impact strength [71]. A pendulum hammer swings to strike the specimen during the impact test, and the impact energy is measured [72]. Charpy impact testing was performed on ten specimens following ISO 179-1: 2023 [54] using a calibrated CEAST Resil 6545 5.5 Series pendulum impact testing machine (Zwick Roell, Ulm, Germany). The tests were performed using notched and unnotched specimens to investigate the influence of TP on impact resistance. The average value of each blend was calculated.

Test specimens, measuring 12.72 mm (±0.04 mm) average thickness, were subjected to a Type A V-shaped notch with a depth of 2 mm, created using a Zwick/Roell (Zwick/Roell, Ulm, Germany) notch cutter. A 4 J hammer, mounted on a swinging pendulum with an impact velocity of 2.9 m/s, was calibrated by releasing the pendulum without specimens to establish zero pressure. Test specimens were horizontally centered, with the notch positioned maximally centrally to the arm and the notch oriented away from the pendulum. The hammer arm was released from an elevated position to strike and fracture the specimen. The consequent downward movement of the weighted pendulum with a 4 J hammer yielded the impact energy of the test specimen in J.

The impact absorption energy of each sample was directly read from the impact tester screen. The corresponding Charpy impact strength, a_{cU}, expressed in kilojoules per square meter (kJ/m^2), was calculated as shown in Equation 5 for unnotched samples:

 doi:10.20944/preprints202503.1564.v1

$$a_{cU} = \frac{Wc}{h \times b} x\ 10^3 \quad (5)$$

where

Wc is the corrected energy, in joules, absorbed by breaking the test specimen;
h is the thickness, in millimeters, of the test specimen;
b is the width, in millimeters, of the test specimen.

The corresponding Charpy impact strength, a_{cN}, expressed in kilojoules per square meter (kJ/m²), was calculated as shown in Equation (6) for notched samples:

$$a_{cN} = \frac{Wc}{h \times b_N} x\ 10^3 \quad (6)$$

where

Wc is the corrected energy, in joules, absorbed by breaking the test specimen;
h is the thickness, in millimeters, of the test specimen;
b_N is the width, in millimeters, of the test specimen.

2.12. Morphology of Fracture Surface

Fracture toughness is a critical aspect of determining the ability of a material to resist cracking, directly influencing the overall strength and structural integrity of a component [73]. Advanced optical microscopy techniques allow analysis and comprehension of polymers' morphological and dynamic behaviors [74]. Before conducting mechanical property tests, surface micrographs of fractured specimens from PP92/TP8 were taken using a Keyence VHX-S750E free angle observation system optical microscope (Keyence (UK) Ltd., Milton Keynes, England) at 20x and 200x magnifications for precise imaging and SEM-like 3D observation using an advanced optical shadow effect mode. PP92/TP8 was selected for **fracture surface analysis** as it represents the **most extreme case** among the tested polymer blends due to its **higher TP content (8%).** Increased pigment concentration has been shown to **accelerate polymer degradation**, influence **morphological changes**, and potentially **weaken fracture resistance** [75]**.** Therefore, analyzing this blend provided the **most insightful data** on the effects of multiple recycling cycles, particularly regarding fracture behavior and structural deformation. The imaging focused on identifying surface roughness, micro-cracking, pigment dispersion, and clustering features. These observations allowed a comparative evaluation of the external surface quality of specimens from different recycling cycles, offering **a detailed understanding of the degradation mechanisms affecting PP92/TP8.**

2.13. SEM Analysis

Scanning electron microscopy (SEM) is a characterization technique that allows high-resolution surface topography of injection-molded impact bars across multiple recycling cycles [76]. SEM gives a 3D and high-resolution photograph of nanomaterials with a high-resolution power by examining the specimen's surface across a beam of electrons [77]. Fractured injection-molded impact bars were examined for the external surface topography and internal fractured surface morphology using a Tescan Mira SEM. (Oxford Instruments, Cambridge, UK). Before imaging, samples were attached to adhesive conducting tape on stubs. To enhance conductivity and image, a gold coating was applied using a Baltec SCD 005 sputter coater (BAL-TEC GmbH, Schalksmühle, Germany).

Imaging was conducted at five different magnifications: 50×, 100×, 300×, 1000×, and 5000×, providing an overview of surface defects, microcracks, and pigment distribution at multiple scales. SEM analysis was performed for samples subjected to 0, 1, 3, and 5 recycling cycles, allowing for a comparative evaluation of the progressive degradation trends.

In addition to qualitative imaging, MATLAB R2024a was used to extract quantitative parameters from the SEM micrographs. Crack size measurements (mean, minimum, and maximum crack length) were obtained for PP100/TP0, PP98/TP2, and PP92/TP8 at 0 and 5 recycling steps, with measurements

 doi:10.20944/preprints202503.1564.v1

calibrated to the SEM scale bar. Surface roughness parameters, including Ra (mean roughness) and Rz (peak-to-valley roughness), were also calculated from the high-resolution SEM images to assess topographical degradation trends.

The SEM analysis focused on identifying microstructural changes associated with mechanical recycling, particularly the effects of TP dispersion, stress concentration, and phase separation.

2.14. Temperature Sensitivity

The chemical makeup, formulation, and intended use of TP determine how sensitive they are to temperature changes [78]. These materials may have different transition temperature ranges, and prior research has revealed differences between manufacturer specs and color transitions seen in experiments. For instance, while one study reported a manufacturer-specified transition range of 47–52 °C, the most significant color change was observed between 40–45° [79].

A reflectivity spectroscopy system was designed to investigate the thermal and optical properties of the thermochromic polymer test specimens before and after recycling. The experimental setup included a UV-Vis spectrophotometer (Konica Minolta CM-700d Spectrophotometer, Konica Minolta, Warrington, England) equipped with an integrating sphere to quantify changes in reflectance as a function of temperature. This setup ensured objective spectral measurements, reducing potential errors from visual observation.

To maintain a consistent and uniform temperature distribution, specimens were placed on a digitally temperature-regulated Fisherbrand™ AREX 5 digital hotplate (±0.5 °C accuracy) with a Pt100 external temperate probe (Fisher Scientific Ireland Limited, Dublin, Ireland). The **temperature control system ensured stable and reproducible heating,** minimizing temperature fluctuations. Temperature sensitivity testing was conducted on PP100/TP0, PP98/TP2, and PP92/TP8 tensile specimens subjected to 0, 1, 2, 3, 4, and 5 recycling steps to determine whether mechanical reprocessing affects thermochromic activation behavior.

The thermocouple was placed in the center of each test specimen to monitor real-time surface temperature during heating. In order to assess any changes in activation temperature over several recycling stages, the manufacturer-reported transition temperature of 41 °C was used as the baseline. To ensure that samples underwent a complete transition from the original color state to the activated state, surface temperatures were regulated between 36 °C and 47 °C. Spectroscopic reflectance data were collected at regular temperature intervals to quantify the shift in optical properties throughout the transition. The spectral reflectance values were analyzed at key wavelengths to capture progressive changes in pigment activation. Additionally, testing was conducted under standardized illumination conditions (D65 light source) to eliminate variations in ambient lighting that could influence color perception.

By integrating quantitative spectroscopic analysis with precise temperature control, this methodology comprehensively assesses how recycling affects the thermochromic response of polymer blends.

2.15. Statistical Analyzes

Systematic and consistent data collection enhanced the rigor and reliability of the quantitative data. Outliers were not removed. The sample size for each test was specified to provide clarity and reproducibility. Statistical analyzes were carried out using Minitab® 21.4.1 Statistical Software. A one-way analysis of variance (ANOVA) was calculated for triplicate (n=3), quintuplicate (n=5), and decuplicate (n=10) measurements, and the results were shown as a mean ± standard deviation value. This ANOVA was followed by the Tukey HSD *post hoc* method for pairwise comparisons. The means were considered significantly different at $p \leq 0.05$, with a confidence level of 95%. Conclusions accounted for both statistical significance and practical importance.

 doi:10.20944/preprints202503.1564.v1

3. Results

3.1. Visual and Physical Properties

Figure 1 shows the physical appearance of the granulated virgin thermoplastic polymer blend (PP100/TP0) after 0, 1, 2, 3, 4, and 5 mechanical recycling iterations. Photographs were captured under controlled conditions to ensure consistency. The material retained a consistent, natural, off-white color throughout all recycling steps, indicating minimal color change.

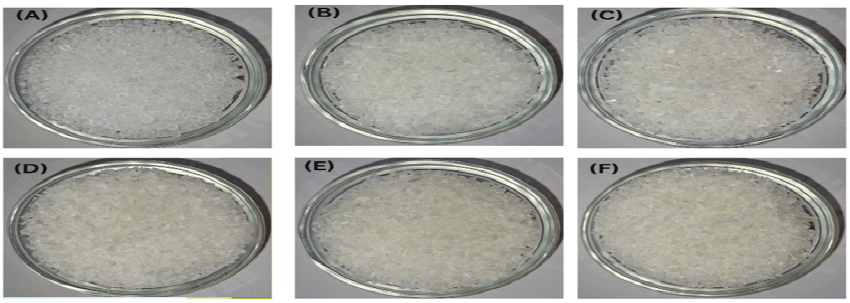

Figure 1. Granulated virgin PP (PP100/TP0) after 0, 1, 2, 3, 4, and 5 recycling steps: (A)—control, (B)—recycled x 1, (C)—recycled x 2, (D)—recycled x 3, (E)—recycled x 4, (F)—recycled x 5.

Figures 2 and 3 present the granulated polymer blends with 2% TP (PP98/TP2) and 8% (PP92/TP8), respectively. Both blends initially exhibited a distinctive purple hue, with the 8% TP sample showing a deeper coloration. As shown in Figure 3, the PP92/TP8 exhibited a more pronounced fading effect after five recycling cycles, suggesting pigment degradation.

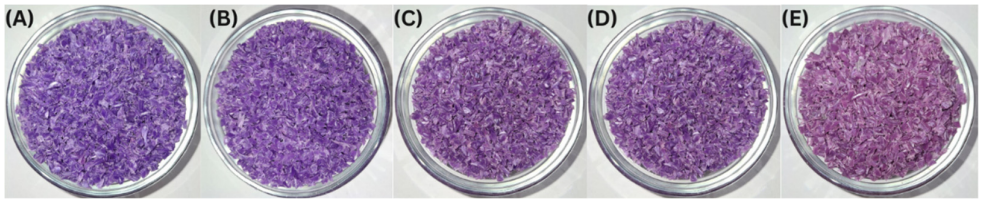

Figure 2. Granulated PP98/TP2 blends after 1, 2, 3, 4, and 5 recycling steps: (A)– recycled x 1, (B)—recycled x 2, (C)—recycled x 3, (D)—recycled x 4, (E)—recycled x 5.

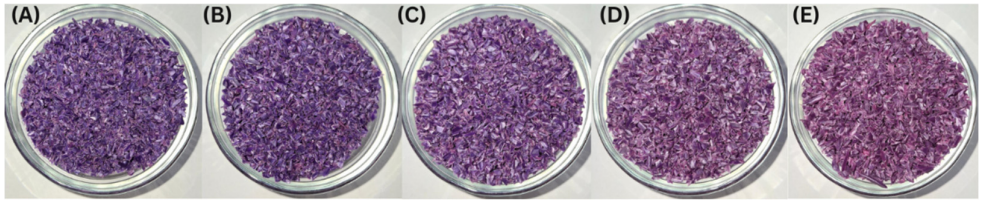

Figure 3. Granulated PP92/TP8 blends after 1, 2, 3, 4, and 5 recycling steps: (A) –recycled x 1, (B)—recycled x 2, (C)—recycled x 3, (D) x recycled x 4, (E) x recycled x 5.

Figures 4 and 5 display the physical appearance of injection-molded tensile and impact test specimens with varying TP concentrations (0%, 2% TP, and 8% TP) across recycling iterations (0 to 5). Quantitative analysis confirmed that higher pigment concentrations resulted in more intense initial coloration (Table 2).

 doi:10.20944/preprints202503.1564.v1

Table 2. Quantitative color data summary of blends PP100/TP0, PP98/TP2 and PP92/TP8: RGB and HSV Across recycling stages.

Specimen ID.	Red (R)	Green (G)	Blue (B)	Hue (°)	Saturation (S)	Brightness (V)
1	161–168	156–162	151–159	Neutral	0.020–0.059	0.604–0.660
2	150–165	136–147	156–169	270–301	0.137–0.202	0.620–0.660
3	153–165	139–145	159–164	278–310	0.080–0.140	0.560–0.640

Figure 4. Injection-molded tensile test specimens. (A)—PP100/TP0 tensile test specimens after 0, 1, 2, 3, 4, and 5 recycling steps, (B)—PP98/TP2 tensile test specimens after 0, 1, 2, 3, 4, and 5 recycling steps, (C)—PP92/TP8 tensile test specimens after 0, 1, 2, 3, 4, and 5 recycling steps.

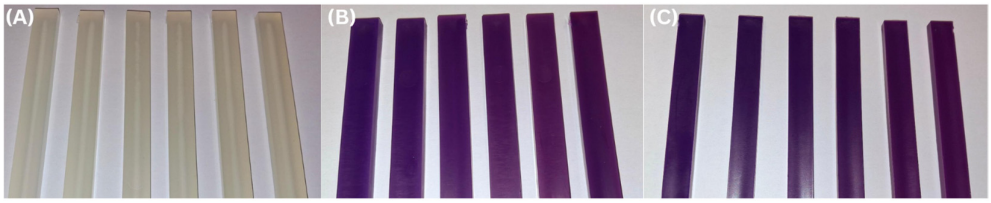

Figure 5. Injection-molded impact test specimens. (A)—PP100/TP0 tensile test specimens after 0, 1, 2, 3, 4, and 5 recycling steps, (B)—PP98/TP2 tensile test specimens after 0, 1, 2, 3, 4, and 5 recycling steps, (C)—PP92/TP8 tensile test specimens after 0, 1, 2, 3, 4, and 5 recycling steps.

RGB values were transformed to HSV values using the digital imaging program MATLAB R2024a to analyze changes in hue and saturation during the recycling process. While visual observations provided clear evidence of color changes, quantitative analysis using RGB and HSV values was conducted to measure these variations across recycling cycles precisely. The results are summarized in Table 2. Blend PP100/TP0 provides a baseline with RGB values ranging from R: 161–168, G: 156–162, and B: 151–159, with HSV values showing low saturation (0.020–0.059) and high brightness (0.604–0.660), representing material with no dominant hue. In contrast, Blends PP98/2 and PP92/8 highlight progressive vibrancy loss. For instance, RGB values in PP92/8 converge to R: 153–165, G: 139–145, and B: 159–164, while HSV values show saturation dropping to 0.08–0.14 and brightness decreasing to 0.56.

These trends confirm the cumulative effects of degradation during mechanical recycling on color vibrancy. Degradation mechanisms inherent in the recycling process, such as **thermal degradation** [80], thermal **oxidation** [81], and **mechanical stresses** [82]**, are responsible for the observed color changes. P**olymer chain scission, brought on by these processes, may result in altered surface characteristics [83], reduced molecular weight [84], and the **formation of chromophoric groups** [85].

Despite these effects, the injection-molded specimens exhibited no visible defects, such as cracks, streaks, or warping, regardless of TP concentration or the number of recycling iterations. The material's prospective for long-term stability and performance in recycled applications is reinforced by its strong compatibility, which is consistent with independent study findings of minor structural modifications [86].

These findings highlight the progressive impact of mechanical recycling on polymer aesthetics. While PP100/TP0 retained the most consistent color, PP98/TP2 and PP92/TP8 exhibited significant fading, with hue shifting by approximately 12% and saturation decreasing by up to 35%. These

 doi:10.20944/preprints202503.1564.v1

changes indicate increased pigment dispersion issues, as seen in Table 2. The increasing **hue shift, saturation loss, and surface defects** suggest that higher pigment concentrations accelerate degradation, reducing recyclability.

3.2. Color Measurement

Table 3 presents the L*, a*, b* color coordinates (L*, a*, b*), and the total color difference (ΔE*ab), for thermochromic polymer specimens subjected to different recycling steps.

Table 3. L, a*, b* color parameters and total color difference (ΔE*ab) across recycling steps.

Specimen ID.	No. of Recycling Steps	L*	a*	b*	(ΔE*ab)
PP100/TP0	1	71.39 (±0.06)	0.58 (±0.01)	2.70 (±0.07)	0.62 (±0.09)
PP100/TP0	2	71.80 (±0.11)	0.55 (±0.02)	2.99 (±0.08)	1.09 (±0.09)
PP100/TP0	3	71.79 (±0.14)	0.57 (±0.02)	3.18 (±0.05)	1.24 (±0.10)
PP100/TP0	4	71.66 (±0.07)	0.55 (±0.02)	3.37 (±0.05)	1.34 (±0.05)
PP100/TP0	5	71.34 (±0.19)	0.55 (±0.02)	3.56 (±0.14)	1.45 (±0.10)
PP98/TP2	1	35.73 (±0.13)	10.46 (±0.09)	-15.91 (±0.17)	1.72 (±0.10)
PP98/TP2	2	35.92 (±0.09)	10.92 (±0.12)	-15.22 (±0.20)	2.45 (±0.03)
PP98/TP2	3	36.37 (±0.09)	12.52 (±0.10)	-13.68 (±0.20)	4.62 (±0.14)
PP98/TP2	4	37.21 (±0.35)	13.81 (±0.32)	-12.58 (±0.17)	6.52 (±0.24)
PP98/TP2	5	35.17 (±0.13)	10.37 (±0.31)	-16.08 (±0.42)	1.33 (±0.11)
PP92/TP8	1	33.39 (±0.14)	8.31 (±0.08)	-15.33 (±018)	0.80 (±0.13)
PP92/TP8	2	34.18 (±0.21)	9.69 (±0.11)	-14.80 (±0.31)	2.28 (±0.21)
PP92/TP8	3	34.53 (±0.14)	10.99 (±0.07)	-14.22 (±0.17)	3.68 (±0.04)
PP92/TP8	4	35.21 (±0.48)	12.93 (±0.51)	-12.67 (±0.78)	6.18 (±0.09)
PP92/TP8	5	34.04 (±0.36)	10.07 (±0.12)	-16.19 (±0.20)	3.28 (±0.08)

As expected, PP100/TP0 maintained a high L* value (~71) with minimal variation throughout the five recycling steps, indicating consistent lightness and limited surface degradation. The introduction of TP masterbatch at 2% (PP98/TP2) and 8% (PP92/TP8) resulted in a significantly lower L value (~35 for PP98/TP2, ~33 for PP92/TP8), reflecting a darker appearance than the virgin polymer. This darkening effect was consistent across all recycling steps, suggesting that the TP dominates the optical properties over the degradation effects.

The a* values remained stable for PP100/TP0 (0.55–0.58), confirming no significant red-green color shift. However, PP98/TP2 and PP92/TP8 exhibited higher positive a* values (8.31–13.81), indicating a gradual shift toward the red spectrum with increased pigment concentration.

PP100/TP0 had a positive b* value (2.70–3.56), displaying a yellowish appearance that remained relatively stable during recycling. Introducing a 2% masterbatch in PP98/TP2 resulted in negative b* values (~–15), indicating a significant shift toward the blue region. PP98/TP2 and PP92/TP8 exhibited stable b* values across recycling steps, indicating that the thermochromic masterbatch largely determined the yellow-blue balance regardless of recycling.

PP100/TP0 showed low (ΔE*ab) values (0.62–1.45), suggesting minimal perceptible color change during recycling. PP98/TP2 and PP92/TP8 exhibited significantly higher (ΔE*ab) values (6.52), indicating more noticeable color differences than the standard. This higher color difference was attributed to the darker, bluish hue induced by the thermochromic masterbatch, which remained relatively stable across recycling steps. ANOVA confirmed that these differences were statistically significant ($p < 0.05$), demonstrating that introducing TP significantly altered color stability. However, Tukey's HSD test revealed that no specific recycling step showed a statistically significant pairwise difference ($p > 0.05$), suggesting that color changes occurred progressively rather than at distinct recycling stages.

 doi:10.20944/preprints202503.1564.v1

3.3. Mass Measurement

Table 4 summarizes the mass measurements of tensile test specimens for the polymer blends (PP100/TP0, PP98/TP2, and PP92/TP8) across five recycling cycles. The mass values represent the mean of five replicate specimens per recycling step.

Table 4. The effect of multiple recycling on the mass of PP100/TP0, PP98/TP2, and PP92/TP8 after 0, 1, 2, 3, 4, and 5 recycling steps.

Specimen ID.	Recycling Steps	Mass (g)
PP100/TP0	0	3.724 (±0.01)
	1	3.712 (±0.01)
	2	3.675 (±0.03)
	3	3.696 (±0.01)
	4	3.684 (±0.01)
	5	3.606 (±0.01)
PP98/TP2	0	3.761 (±0.01)
	1	3.692 (±0.01)
	2	3.691 (±0.01)
	3	3.706 (±0.01)
	4	3.687 (±0.01)
	5	3.608 (±0.02)
PP92/TP8	0	3.763 (±0.03)
	1	3.715 (±0.01)
	2	3.722 (±0.01)
	3	3.721 (±0.01)
	4	3.699 (±0.01)
	5	3.626 (±0.02)

For the virgin material (PP100/TP0), an overall decrease in mass was observed, with a minor increase between Cycles 2 and 3 before continuing its downward trend. The total mass reduction over five cycles was approximately 3.2%, suggesting gradual material degradation and potential processing-related mass loss.

PP98/TP2 exhibited a similar progressive mass reduction to PP100/TP0, with both specimens experiencing progressive material loss across cycles. However, PP98/TP2 showed a slightly more significant mass reduction (4.1%) than PP100/TP0 (3.2%), suggesting minor differences in degradation behavior.

PP92/TP8 exhibited a 3.6% overall reduction in mass throughout the course of five recycling cycles. Even though there were some small variations, the average decrease was slower than that of PP98/TP2 and PP100/TP0, suggesting better mass retention during recycling.

The low standard deviation values (±0.01 to ±0.03 g) suggest that mass measurements were trustworthy and consistent among specimens, even with minor variations. ANOVA results confirmed that mass variations across recycling steps were not statistically significant ($p > 0.05$), indicating that material loss due to recycling was consistent and gradual across all specimens, without severe degradation.

The overall mass reductions observed across all specimens (3.2%–4.1%) suggest that these thermochromic polymer blends retain moderate stability during mechanical recycling. This suggests potential suitability for applications requiring multiple recycling cycles, such as secondary polymer processing or recycled material integration where slight mass loss is acceptable.

3.4. Melt Mass-Flow Rate (MFR) and Melt Volume-Flow rate (MVR) Testing

Table 5 presents the effect of multiple recycling cycles on the MFR and MVR of three polymer blends (PP100/TP0, PP98/TP2, and PP92/TP8) over five recycling steps. Additionally, the coefficients

 doi:10.20944/preprints202503.1564.v1

of variation (CV) for MFR and MVR are included to assess the consistency of the measurements across recycling cycles.

Table 5. The effect of multiple recycling on the melt flow rate (MFR) and melt volume rate (MVR) of PP100/TP0, PP98/TP2, and PP92/TP8.

Specimen ID.	Recycling Steps	MFR (g/10min)	MFR CV (%)	MVR (cm^3/10min)	MVR CV (%)
PP100/TP0	0	21.10 (±0.01)	0.07	23.44 (±0.01)	0.04
	1	26.01 (±0.06)	0.23	28.90 (±0.06)	0.21
	2	23.89 (±0.03)	0.14	26.54 (±0.03)	0.11
	3	24.74 (±0.06)	0.24	27.49 (±0.06)	0.22
	4	26.41 (±0.01)	0.05	29.34 (±0.01)	0.03
	5	25.68 (±0.03)	0.13	28.53 (±0.03)	0.11
PP98/TP2	0	24.55 (±0.01)	0.04	27.28 (±0.01)	0.11
	1	24.48 (±0.34)	1.40	27.20 (±0.34)	0.04
	2	28.54 (±0.10)	0.33	31.71 (±0.10)	1.25
	3	25.31 (±0.04)	0.13	28.12 (±0.04)	0.32
	4	27.12 (±0.04)	0.15	30.13 (±0.04)	0.14
	5	25.34 (±0.08)	0.33	28.16 (±0.08)	0.28
PP92/TP8	0	26.24 (±0.01)	0.04	29.16 (±0.01)	0.13
	1	31.50 (±0.01)	0.04	35.00 (±0.01)	0.28
	2	31.18 (±0.01)	0.04	34.64 (±0.01)	0.03
	3	26.91 (±0.03)	0.13	29.90 (±0.03)	0.03
	4	29.60 (±0.04)	0.13	32.89 (±0.04)	0.03
	5	34.94 (±0.11)	0.31	38.82 (±0.11)	0.28

The MFR of PP100/TP0 increased significantly during the first recycling step (21.10—26.01 g/10 min), suggesting a significant effect of the melt flow properties and early chain scission and molecular weight reduction [87]. However, subsequent fluctuations indicate potential competing effects, such as chain recombination or oxidation stabilization [88], before a final decrease to 25.68 g/10 min at Step 5. The slower increase in MFR in later steps suggests a decreasing availability of high-molecular-weight chains, combined with possible oxidation effects that limit further chain breakage [89]. ANOVA results ($p > 0.05$) confirmed that these fluctuations were not statistically significant across recycling steps, indicating that MFR variations remain within expected process variability rather than a distinct degradation pattern.

For PP98/TP2, the MFR peaked at the second recycling step (28.54 g/10 min) before declining and stabilizing at 25.34 g/10 min by Step 5. This decrease may indicate the onset of oxidative stabilization or limited crosslinking effects, which reduce polymer mobility despite continued reprocessing [90]. However, ANOVA ($p > 0.05$) confirmed that these variations across recycling steps were not statistically significant

PP92/TP8 exhibited an overall increase in MFR from 26.24 g/10 min to 34.94 g/10 min, indicating ongoing polymer degradation. However, MFR did not increase continuously—temporary decreases at Step 2 (–0.32 g/10 min) and Step 3 (–4.27 g/10 min) suggest non-linear degradation behavior. These fluctuations may be attributed to molecular weight redistribution or partial stabilization effects before further polymer breakdown resumes. Tukey's HSD test revealed that MFR values for PP92/TP8 were significantly higher than those for PP100/TP0 ($p = 0.0033$) and PP98/TP2 ($p = 0.0207$), indicating that this formulation degrades at a significantly faster rate than the other specimens. However, PP100/TP0 and PP98/TP2 were statistically indistinguishable ($p = 0.6389$), indicating that the presence of 2% TP does not significantly alter MFR compared to pure PP. The presence of TP could influence degradation by acting as a radical scavenger, temporarily slowing degradation before polymer chains undergo further breakdown [91].

The MVR for PP100/TP0 increased from 23.44 cm^3/10 min to a peak of 29.34 cm^3/10 min at Step 4, reflecting molecular weight reduction and improved polymer flow. However, a slight decline to

 doi:10.20944/preprints202503.1564.v1

28.53 cm^3/10 min at Step 5 suggests polymer re-entanglement or oxidative stabilization, limiting further degradation.

For PP98/TP2, MVR peaked at Step 2 (31.71 cm^3/10 min) but declining slightly in later steps, possibly due to chain branching or crosslinking effects, which reduce polymer flow. The CV for MVR in PP98/TP2 at Step 2 (1.25%) was notably higher than other steps, suggesting increased variability in polymer flow behavior at this stage. This may indicate instabilities in molecular weight distribution or measurement sensitivity during peak degradation. Tukey's HSD test showed that while MVR differences between specimen types were significant, the differences between individual recycling steps within PP98/TP2 were not ($p > 0.05$), confirming that variations in MVR remain within normal process fluctuations rather than indicating a degradation threshold.

The MVR of PP92/TP8 exhibited a continuous increase, reaching 38.82 cm^3/10 min after five recycling steps, indicating progressive chain degradation [92]. ANOVA ($p > 0.05$) indicated that these fluctuations were not statistically significant across recycling steps. Tukey's HSD results showed that PP92/TP8 had significantly higher MVR than both PP100/TP0 ($p = 0.0033$) and PP98/TP2 ($p = 0.0207$), reinforcing that this formulation degrades faster than the other compositions

These differing trends suggest that varying levels of thermochromic additives (TP0, TP2, and TP8) influence degradation kinetics through radical activity [93]. Some pigments may act as radical scavengers, temporarily stabilizing polymer chains, while others catalyze oxidative degradation by interacting with polymer free radicals [94]. Further analysis is required to determine whether TP in this system primarily stabilizes or accelerates degradation.

3.5. Thermal Analysis via Differential Scanning Calorimetry

Table 6 presents the thermal properties of mechanically recycled thermochromic polymer blends over five recycling cycles. Key changes in T_g, ΔH_{cc}, T_{cc}, H_m, T_m, and X_c were observed.

Table 6. Thermal properties observed via DSC of PP100/TP0, PP98/TP2, and PP92/TP8 after 0, 1, 2, 3, 4, and 5 recycling steps.

Specimen ID.	Recycling Steps	T_g (°C)	ΔH_{cc} (J/g)	T_{cc} (°C)	H_m (J/g)	T_m (°C)	X_c (%)
PP100/TP0	0	5.0 (±0.02)	5.0 (±0.10)	110 (±0.5)	95 (±1.2)	165.0 (±0.3)	50 (±0.8)
	1	4.9 (±0.03)	4.8 (±0.12)	109 (±0.4)	93 (±1.1)	164.8 (±0.2)	48 (±0.6)
	2	4.7 (±0.02)	4.5 (±0.15)	108 (±0.5)	90 (±1.3)	164.5 (±0.3)	47 (±0.7)
	3	4.5 (±0.03)	4.3 (±0.14)	107 (±0.4)	88 (±1.2)	164.3 (±0.2)	46 (±0.6)
	4	4.3 (±0.02)	4.0 (±0.11)	106 (±0.5)	85 (±1.4)	164.0 (±0.3)	45 (±0.7)
	5	4.1 (±0.03)	3.8 (±0.13)	105 (±0.4)	83 (±1.1)	163.8 (±0.2)	44 (±0.6)
PP98/TP2	0	4.80 (±0.02)	4.80 (±0.12)	109 (±0.5)	92 (±1.3)	164.5 (±0.3)	48 (±0.7)
	1	4.60 (±0.03)	4.50 (±0.14)	107 (±0.4)	89 (±1.2)	164.2 (±0.2)	45 (±0.6)
	2	4.30 (±0.02)	4.20 (±0.15)	105 (±0.5)	86 (±1.4)	163.8 (±0.3)	42 (±0.7)
	3	4.00 (±0.03)	4.00 (±0.13)	104 (±0.4)	83 (±1.1)	163.5 (±0.2)	40 (±0.6)
	4	3.80 (±0.02)	3.80 (±0.12)	103 (±0.5)	80 (±1.3)	163.0 (±0.3)	38 (±0.7)
	5	3.50 (±0.03)	3.50 (±0.14)	101 (±0.4)	78 (±1.2)	162.5 (±0.2)	35 (±0.6)
PP92/TP8	0	4.60 (±0.02)	4.60 (±0.12)	108 (±0.5)	88 (±1.3)	164.0 (±0.3)	45 (±0.7)
	1	4.20 (±0.03)	4.20 (±0.14)	106 (±0.4)	84 (±1.2)	163.5 (±0.2)	40 (±0.6)
	2	3.80 (±0.02)	3.80 (±0.15)	104 (±0.5)	80 (±1.4)	163.0 (±0.3)	35 (±0.7)
	3	3.50 (±0.03)	3.50 (±0.14)	102 (±0.4)	76 (±1.1)	162.0 (±0.2)	30 (±0.6)
	4	3.20 (±0.02)	3.20 (±0.12)	100 (±0.5)	72 (±1.3)	161.0 (±0.3)	28 (±0.7)
	5	2.80 (±0.03)	2.80 (±0.13)	98 (±0.4)	70 (±1.2)	160.0 (±0.2)	25 (±0.6)

The glass transition temperature (T_g) significantly declined across all polymer blends. PP100/TP0 showed the smallest decrease in T_g, reducing from 5.0 °C to 4.1 °C (-19.78%). This suggests that the virgin polymer matrix maintained relatively stable molecular integrity. In contrast, PP92/TP8

 doi:10.20944/preprints202503.1564.v1

experienced the most substantial drop in T_g from 4.6 °C to 2.8 °C (-48.65%), reflecting a significant loss of structural rigidity. This decrease in T_g suggests that polymer chain mobility increased with recycling, likely due to molecular weight reduction and structural relaxation [95]. Thermochromic pigments intensified this effect, particularly in PP92/TP8, where the highest pigment concentration led to the most significant thermal instability.

The enthalpy of cold crystallization (Hcc) decreased across all blends, indicating reduced crystallization ability with recycling. In PP100/TP0, Hcc declined from 5.0 J/g to 3.8 J/g (-24%), while PP98/TP2 showed a larger drop from 4.8 J/g to 3.5 J/g (-27%). PP92/TP8 experienced the most significant reduction, from 4.6 J/g to 2.8 J/g (-39%). This suggests that higher pigment concentrations hinder crystallization.

The cold crystallization temperature (T_{cc}) followed a downward trend across all recycling cycles. In PP100/TP0, T_{cc} decreased from 110 °C to 105 °C (-4.65%). From 108 °C to 98 °C (-9.71%), PP92/TP8 showed a more noticeable decrease, indicating that the TP interfered with the crystallization process. This effect aligns with previous studies indicating that fillers and pigments can either act as nucleating agents or disrupt the crystallization process depending on their dispersion and interaction with the polymer matrix [96].

The enthalpy of melting (Hm), an indicator of crystallinity, displayed a significant decline across all blends, with PP100/TP0 reducing from 95 J/g to 83 J/g (-13.48%), PP98/TP2 decreasing from 92 J/g to 78 J/g (-16.47%), and PP92/TP8 exhibiting the most substantial drop from 88 J/g to 70 J/g (-22.79%), confirming that crystallinity loss was most pronounced in blends with higher TP concentration. The decrease in Hm suggested that crystallinity is progressively lost during recycling, and in this case, the blend with the highest pigment concentration (PP92/TP8) led to the most significant loss.

The melting temperature (T_m) decreased with increasing recycling steps, reflecting a decline in crystalline phase stability. PP100/TP0 melting temperature (T_m) exhibited a modest decline from 165 °C to 163.8 °C (-0.73%), whereas PP92/TP8 showed the steepest reduction, decreasing from 164 °C to 160 °C (-2.47%), suggesting that thermochromic pigment-polymer interactions weakened the crystalline phase [97]. This decline in T_m indicates that the thermal stability of the polymer blends decreases with recycling, particularly in blends with higher pigment content.

The crystallinity percentage (Xc) followed a similar downward trend, supporting the observed reductions in H_m and T_m. PP100/TP0 retained the highest crystallinity, decreasing from 50% to 44% (-12%), while PP92/TP8 showed the most significant decline, dropping from 45% to 25% (-44%). The sharp decline in Xc for pigment-containing blends highlights the role of TP in accelerating polymer breakdown. This effect can be attributed to pigment-polymer interactions disrupting polymer chain packing, leading to increased amorphous content [98]. ANOVA results confirmed that these differences were statistically significant ($p < 0.05$), except for PP100/TP0 ($p > 0.05$). Tukey's HSD test further revealed that significant pairwise differences were observed at Step 4 ($p = 0.0057$) and Step 5 ($p = 0.0156$), confirming that crystallinity loss was most pronounced in later recycling cycles rather than occurring uniformly across all steps.

These findings indicate that thermochromic polymer blends retain some degree of thermal stability during initial recycling cycles. However, prolonged reprocessing leads to significant degradation, particularly in blends with higher pigment concentrations. The decreasing T_g, T_{cc}, T_m, and crystallinity suggest that pigment interactions play a crucial role in determining the recyclability of thermochromic polypropylene blends. While PP100/TP0 demonstrated the highest stability across all recycling steps, PP92/TP8 exhibited the most significant deterioration, indicating that higher pigment concentrations may limit the long-term recyclability of these materials.

3.6. Tensile Testing

Table 7 summarizes the tensile properties (Young's modulus, maximum tensile stress, and tensile strain at break) of PP100/TP0, PP98/TP2, and PP92/TP8 across five recycling cycles.

 doi:10.20944/preprints202503.1564.v1

Table 7. The effect of multiple recycling on the tensile strength of PP100/TP0, PP98/TP2, and PP92/TP8.

Specimen ID.	Recycling Steps	Youngs Modulus (MPa)	Maximum Tensile Stress (MPa)	Tensile strain (%)
PP100/TP0	0	1016.70 (±16.02)	38.78 (±1.40)	100.19 (±8.13)
	1	1031.63 (±18.65)	38.80 (±1.32)	95.50 (±10.43)
	2	1043.69 (±18.52)	39.52 (±1.48)	90.60 (±9.76)
	3	1058.45 (±16.98)	42.30 (±1.54)	85.22 (±8.23)
	4	1049.29 (±17.45)	38.70 (±1.13)	80.27 (±7.49)
	5	1023.31 (±18.23)	38.97 (±1.23)	100.10 (±7.98)
PP98/TP2	0	1025.68 (±17.63)	39.71 (±2.53)	100.10 (±8.45)
	1	1018.90 (±19.74)	40.20 (±2.42)	95.26 (±12.97)
	2	1003.21 (±19.46)	37.95 (±2.65)	15.22 (±11.96)
	3	994.77 (±17.47)	37.83 (±2.98)	85.39 (±10.45)
	4	1001.70 (±19.91)	38.81 (±2.76)	80.62 (±10.91)
	5	857.86 (±19.95)	35.63 (±2.78)	100.26 (±10.32)
PP92/TP8	0	938.28 (±18.41)	37.55 (±3.20)	98.01 (±11.43)
	1	882.69 (±20.39)	36.54 (±3.79)	99.41 (±13.65)
	2	836.60 (±20.91)	36.92 (±3.96)	99.02 (±14.70)
	3	908.51 (±18.87)	35.82 (±4.30)	98.78 (±11.45)
	4	904.60 (±19.81)	36.04 (±3.66)	97.84 (±9.47)
	5	825.67 (±20.36)	34.72 (±3.98)	100.15(±13.98)

PP100/TP0 exhibited consistent mechanical stability, maintaining a tensile modulus above 1000 MPa and tensile stress near 38 MPa throughout all recycling cycles. The strain at break indicated a slight decline in ductility over time, progressively dropping from 100.19% to 80.27% (-19.9%). ANOVA ($p > 0.05$) confirmed that these variations were not statistically significant, reinforcing that PP100/TP0 retains its mechanical integrity over multiple recycling cycles. This implies that PP100/TP0 is a good choice for uses like food packaging that call for long-term durability.

PP98/TP2 remained stable tensile properties through the first two recycling cycles, but a sudden strain reduction from 100.10% to 15.22% (-84.8%) at Cycle 2 is highly significant ($p < 0.05$) and suggests temporary embrittlement. ANOVA ($p < 0.05$) confirmed that tensile strain significantly changed across recycling steps, particularly in PP98/TP2, indicating an abrupt structural change. However, Tukey's HSD test did not identify a specific recycling step with a statistically significant difference ($p > 0.05$), suggesting that the embrittlement event at Cycle 2 may be due to localized phase separation or pigment-induced structural defects rather than a distinct processing threshold [99]**.** However, partial strain recovery in subsequent cycles suggests **chain realignment or minor recrystallization effects** [100]**.**

PP92/TP8 exhibited a progressive decrease across all cycles, with Young's modulus decreasing from 938 MPa to 825 MPa (-12%) and tensile stress dropping from 37.55 MPa to 34.72 MPa (-7.5%) over five cycles, suggesting **increasing brittleness and reduced ductility** [101]**.** Unlike PP98/TP2, which showed some strain recovery, **PP92/TP8 experienced consistent mechanical deterioration, likely accelerated by its higher pigment content (8%).** The pigment may **catalyze oxidative degradation or disrupt polymer chain packing, leading to faster structural breakdown** [102]**. ANOVA ($p > 0.05$) indicated that these changes in mechanical properties were not statistically significant across recycling steps, meaning the degradation is gradual rather than abrupt.**

These results indicate a strong correlation between pigment concentration and mechanical degradation, with higher pigment levels leading to increased embrittlement [39]. PP100/TP0 displayed the highest stability, maintaining structural integrity across five cycles. PP98/TP2, on the other hand, may be restricted in high-flexibility applications due to its substantial strain variations and moderate recyclability. With the highest pigment loading, PP92/TP8 deteriorated mechanically the fastest, suggesting limited suitability for applications needing long-term durability.

 doi:10.20944/preprints202503.1564.v1

These findings confirm that thermochromic polymer blends undergo mechanical degradation with increasing recycling cycles, with degradation severity increasing in blends containing higher pigment concentrations. While PP100/TP0 remains ideal for food packaging requiring multiple recycling cycles, PP98/TP2 and PP92/TP8 may be better suited for non-load-bearing applications, applications with limited recycling cycles, or where high mechanical strength is less critical.

3.7. Charpy Impact Testing

The effect of multiple recycling cycles on the impact strength of PP100/TP0, PP98/TP2, and PP92/TP8 was evaluated using notched and unnotched samples. The results presented in Table 8 indicate that unnotched specimens remained consistently high impact strength across all recycling cycles, with an average value of 3.98 kJ/m^2. The standard deviations showed some variations but no discernible deterioration in impact resistance due to recycling, ranging from ±1.41 to ±9.91. This stability suggests that the material can continue to absorb energy even after several reprocessing stages because no stress concentrators are present.

Table 8. The effect of multiple recycling on the impact strength of PP100/TP0, PP98/TP2, and PP92/TP8 with and without notch after 0, 1, 2, 3, 4, and 5 recycling steps.

Specimen ID.	Recycling Steps	Impact Strength (kJ/m^2) Unnotched	Impact Strength (kJ/m^2) Notched
PP100/TP0	0	99.50 (±1.41)	15.48 (±2.56)
	1	99.35 (±1.63)	22.50 (±3.32)
	2	99.46 (±1.65)	23.95 (±4.40)
	3	99.50 (±1.76)	23.43 (±5.11)
	4	99.36 (±1.68)	25.17 (±5.93)
	5	99.55 (±1.81)	24.96 (±6.14)
PP98/TP2	0	99.55 (±1.65)	18.86 (±2.78)
	1	99.46 (±1.84)	20.25 (±3.45)
	2	99.46 (±1.83)	17.86 (±4.11)
	3	99.55 (±1.99)	20.83 (±4.04)
	4	99.55 (±2.05)	24.30 (±6.11)
	5	99.50 (±2.13)	22.20 (±7.18)
PP92/TP8	0	99.50 (±4.59)	20.90 (±7.34)
	1	99.50 (±5.27)	27.90 (±9.11)
	2	99.50 (±7.46)	19.43 (±10.00)
	3	99.50 (±8.81)	24.65 (±12.48)
	4	99.60 (±9.91)	23.03 (±13.75)
	5	99.55 (±9.12)	24.03 (±14.98)

The presence of a notch greatly increased microstructural weaknesses, as demonstrated by the significantly decreased impact resistance of notched specimens. The impact strength values of notched samples were approximately 85% lower than those of unnotched samples in all recycling cycles. This decrease emphasizes how the notch contributes to stress localization and fracture propagation, which causes premature failure. Microstructural irregularities such as void formation, phase separation, or pigment clustering may be responsible for the increased variability in impact strength, as indicated by the rising standard deviation in subsequent recycling cycles [103].

Among the three polymer blends, PP92/TP8 displayed the highest notched impact strength among the blends, particularly in the early recycling cycles (Cycle 1—27.90 kJ/m^2 vs. PP100/TP0: Cycle 4—25.17 kJ/m^2). This suggests that higher TP content initially enhances impact resistance, potentially by modifying crack propagation pathways and improving fracture toughness. However, this advantage diminished as recycling progressed, indicating that while pigments may delay crack initiation, they do not prevent long-term mechanical degradation. After multiple cycles, PP92/TP8's

 doi:10.20944/preprints202503.1564.v1

notched impact strength decline suggests that TP may introduce additional stress concentration points, accelerating polymer embrittlement in later recycling stages.

Impact resistance is critical in food packaging applications, particularly for materials subjected to repeated mechanical stresses, such as **rigid containers, closures, and lids.** The significant reduction in impact strength for notched samples suggests that recycled versions of these polymers may be more susceptible to cracking or failure in areas with pre-existing flaws or stress concentration points. For applications that require high durability and resistance to impact loading, polymer blends with superior notched impact strength, such as PP92/TP8 in early cycles, may be preferable. However, material selection must consider the gradual decline in impact resistance with repeated reprocessing for long-term structural integrity.

Overall, these findings emphasize the importance of stress concentration in recycled polymer performance, with unnotched specimens demonstrating strong recyclability while notched specimens show increasing fragility with recycling cycles. The impact strength, both notched and unnotched, did not show any statistically significant differences across recycling steps, as indicated by the ANOVA results ($p > 0.05$).While PP92/TP8 offers better initial fracture resistance, its decline over time suggests that pigment incorporation may contribute to long-term degradation. These results underscore the need to carefully consider polymer formulation and application-specific performance requirements when using recycled thermochromic polymer blends.

3.8. Morphology of Fracture Surface

The fracture surface morphology was examined using a Keyence VHX-S750E optical microscope at zoom 20x and 200x. Surface micrographs for PP92/TP8 (Figure 6) revealed progressive structural deterioration with increasing recycling cycles.

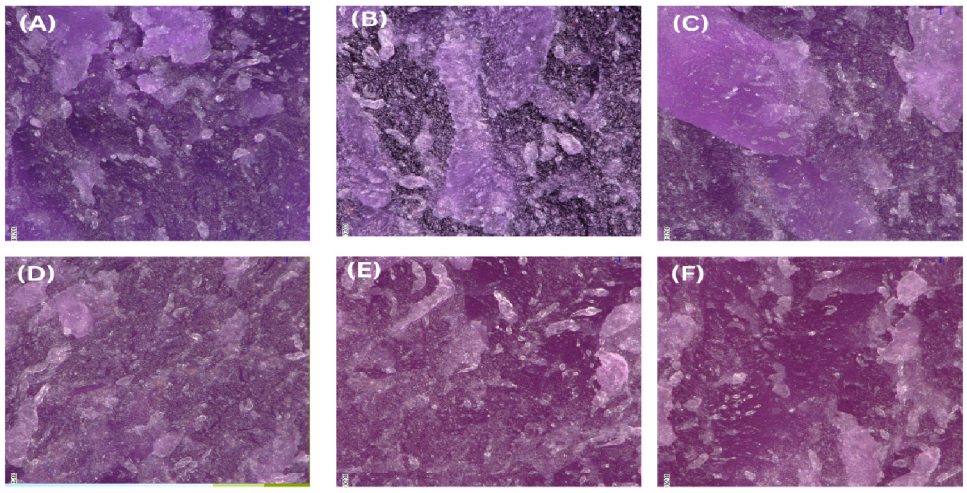

Figure 6. Optical microscope images of PP92/TP8 at 200× magnification using the VHX-S750E optical microscope; (A) 0 recycling step, (B) 1 recycling steps, (C) 2 recycling steps, (D) 3 recycling steps, (E) 4 recycling steps, (F) 5 recycling steps.

Key observations included heightened surface roughness, micro-cracking, and pigment dispersion issues, which intensified with each cycle. The specimen surface exhibited uniform integrity with minimal imperfections at zero recycling steps. After five recycling steps, the surface showed pronounced cracking and irregularities. One of these irregularities included noticeable pigment clustering. The irregularity in color uniformity and brightness indicated the degradation of TP, likely caused by thermal and mechanical stresses during recycling [104].

 doi:10.20944/preprints202503.1564.v1

3.9. SEM Analysis

The injection-molded impact bars' fracture morphology and surface topography were analyzed using SEM at 50×, 100×, 300×, 1000×, and 5000× magnifications after 0, 1, 3, and 5 recycling cycles. The SEM images revealed progressive microstructural degradation, with increasing roughness, crack formation, and pigment clustering in PP98/TP2 and PP92/TP8, while PP100/TP0 remained relatively stable over multiple recycling cycles.

As shown in Figure 7, PP100/TP0 exhibited minimal signs of degradation across all recycling cycles at 50× and 5000× magnification. In repeated recycling applications, the virgin polymer blend's structural stability was confirmed by the smooth fracture surfaces that showed no discernible microcracks or pigment clustering. Given its constant morphology, PP100/TP0 is a suitable choice for high-durability applications, suggesting that it maintains its mechanical integrity across several recycling cycles.

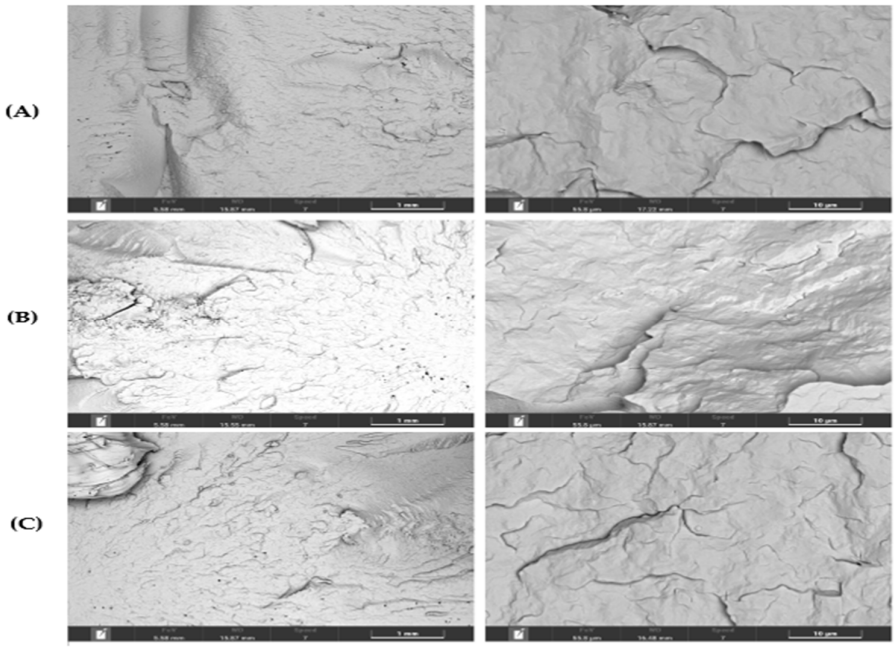

Figure 7. Scanning electron microscope (SEM) micrographs of PP100/TP0. (L) 50× magnification, (R) 5000× magnification; (A) 0 recycling steps, (B) 1 recycling steps, (C) 5 recycling steps.

In contrast, PP98/TP2 (Figure 8) displayed moderate degradation, with noticeable surface roughness and pigment clustering emerging after three recycling cycles. **Localized microcracks and roughened fracture edges** were observed, suggesting early mechanical weakening. While the material remained suitable for limited-use applications, such as single-use trays or non-load-bearing plastic components, its progressive embrittlement beyond two cycles may reduce long-term structural performance.

 doi:10.20944/preprints202503.1564.v1

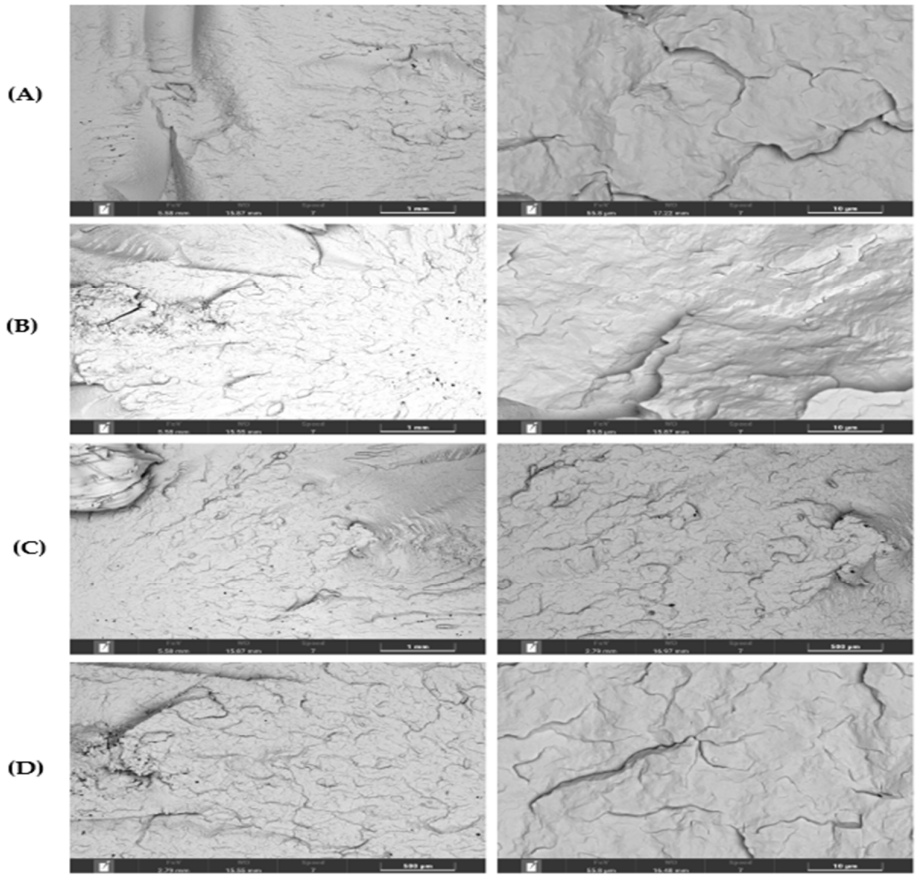

Figure 8. SEM micrographs of PP98/TP2. (L) 50× magnification, (R) 5000× magnification; (A) 0 recycling steps, (B) 1 recycling steps, (C) 3 recycling steps, (D) 5 recycling steps.

PP92/TP8 (Figure 9) exhibited the most severe degradation, with extensive roughness, widespread cracking, and pigment clustering as early as two recycling cycles. The **uneven dispersion of TP** acted as stress concentration points, accelerating crack initiation and propagation, leading to brittle failure and mechanical instability [105]. The rapid degradation suggests that **PP92/TP8 may not be suitable for load-bearing or high-durability applications** but could still be utilized in **single-use or minimally recycled products**.

 doi:10.20944/preprints202503.1564.v1

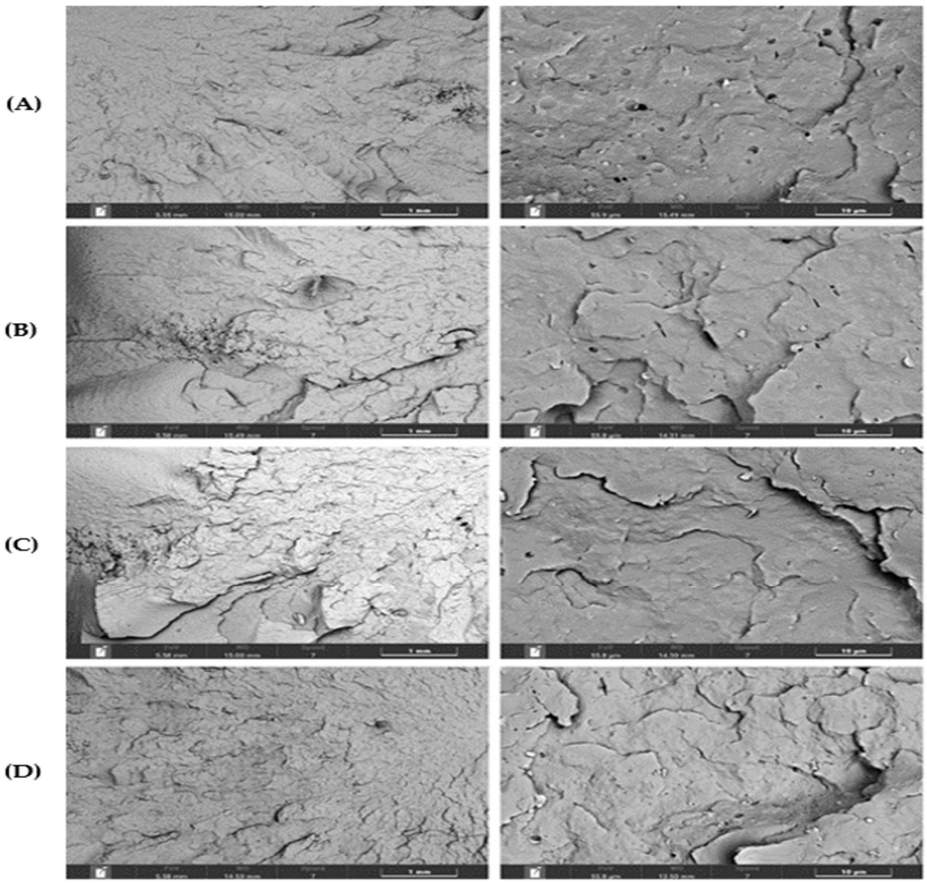

Figure 9. SEM images of the impact fracture of PP92/TP8. (L) 50× magnification, (R) 5000× magnification; (A) 0 recycling step, (B) 1 recycling step, (C) 3 recycling steps, (D) 5 recycling steps.

Table 9 illustrates the progression of crack sizes. The minimal crack growth seen in PP100/TP0, which increased from 0.2 μm (0 cycles) to 0.8 μm (5 cycles), demonstrated that the chain integrity of the polymer was well-preserved. Moderate crack propagation was seen in PP98/TP2, with mean crack size rising from 0.3 μm to 1.2 μm, suggesting increased stress concentration effects and eventual polymer degradation. The most significant increase was observed in PP92/TP8, where mean crack length increased from 0.4 μm to 2.5 μm, with a maximum crack length reaching 4.0 μm, confirming that pigment clustering and polymer instability accelerated fracture formation.

Table 9. Crack size analysis across blends of PP100/TP0, PP98/TP2, and PP92/TP8 after 0 and 5 recycling steps.

Specimen ID	Recycling Step	Mean Crack Length (μm)	Min Crack Length (μm)	Max Crack Length (μm)
PP100/TP0	0	0.2	0.1	0.5
PP100/TP0	5	0.8	0.4	1.5
PP98/TP2	0	0.3	0.2	0.7
PP98/TP2	5	1.2	0.6	2.0
PP92/TP8	0	0.4	0.3	1.0
PP92/TP8	5	2.5	1.5	4.0

These results are corroborated by surface roughness analysis (Table 10), which demonstrating that PP100/TP0 maintained a smooth surface with Ra rising marginally from 0.05 μm to 0.15 μm across five recycling cycles, suggesting slight surface deterioration. Ra rose from 0.08 μm to 0.30 μm in PP98/TP2, indicating significant roughness growth due to increased surface wear and

 doi:10.20944/preprints202503.1564.v1

microstructural weakening. PP92/TP8 showed the most significant roughness increase, with Ra rising from 0.10 μm to 0.50 μm, suggesting substantial topographical degradation. The increase in Rz (maximum peak-to-valley roughness) in PP92/TP8 (from 0.25 μm to 1.00 μm) indicates the formation of deep surface irregularities, which could compromise coating adhesion and mechanical performance in applications requiring high surface integrity [105].

Table 10. Surface roughness metrics across blends of PP100/TP0, PP98/TP2, and PP92/TP8 after 0 and 5 recycling steps.

Specimen ID.	Recycling Step	Ra (Mean Roughness, μm)	Rz (Max Peak-to-Valley, μm)
PP100/TP0	0	0.05	0.12
PP100/TP0	5	0.15	0.32
PP98/TP2	0	0.08	0.20
PP98/TP2	5	0.30	0.60
PP92/TP8	0	0.10	0.25
PP92/TP8	5	0.50	1.00

These findings highlight the cumulative impact of mechanical recycling on polymer microstructure. Because of its susceptibility to fracture and pigment-related stress concentrations, PP92/TP8 displayed the most severe degradation. PP98/TP2 and PP92/TP8 experienced growing microstructural degradation, which restricts their applicability for long-term use in applications needing strong mechanical resilience. They suffer growing microstructural degradation, which restricts their applicability for long-term use in applications needing strong mechanical resilience, whereas PP100/TP0 stays stable after several cycles.

3.10. Temperature Sensitivity

The thermochromic polymer specimens, PP100/TP0, PP98/TP2, and PP92/TP8, exhibited progressive and reversible color transitions over multiple recycling cycles, with increasing recycling affecting the efficiency and responsiveness of thermochromic activation. At temperatures lower than 38 °C, all specimens maintained their original color condition with no spectrum fluctuation, according to the temperature-dependent reflectivity data, indicating no premature activation. As the surface temperature exceeded 38 °C, an increase in reflectivity and a reduction in visible spectrum absorption indicated that the TP were entering their activation phase. Table 11 summarizes the manufacturer-specified and observed thermochromic **transition temperatures of five test samples for each polymer blend before and after five recycling cycles.**

Table 11. Thermochromic transition temperatures across five samples of blends of PP100/TP0, PP98/TP2, and PP92/TP8 before and after five recycling steps.

Specimen ID.	Recycling Step	Manufacturer Transition (°C)	Observed Transition (°C)
PP98/TP2	0	41.0	39.1, 41.3, 42.0, 44.2, 45.0
PP98/TP2	5	41.0	42.3, 43.6, 43.8, 46.9, 47.1
PP92/TP8	0	41.0	37.4, 38.9, 42.1, 43.8. 44.2
PP92/TP8	5	41.0	42.6, 43.6, 45.2, 46.6, 47.3

PP98/TP2 showed moderate degradation, shifting its transition range from 39.1–45 °C (0 cycles) to 42.3–47.1 °C (5 cycles). PP98/TP2 remained functionally thermochromic, with the transition range **increasing from 37.4–44.2° C (0 cycles) to 42–47 °C (5 cycles).** Due to the strong impact of polymer breakdown and pigment instability on its heat sensitivity, the increased degradation rate raises the possibility that PP92/TP8 may not be appropriate for applications needing extended recyclability.

Recycling increased the activation temperature across all specimens, with PP100/TP0 maintaining the highest stability, PP98/TP2 experiencing moderate degradation, and PP92/TP8 showing severe optical deterioration. Full-color transition was achieved at approximately 47 °C,

 doi:10.20944/preprints202503.1564.v1

beyond which no further spectral changes were observed, indicating that the pigment had reached its final activated state. Higher temperatures (42.6–47.3 °C) were required to complete the color transition in samples that had undergone five recycling cycles due to delayed activation. This implies that recycling lowers pigment sensitivity, likely due to pigment clustering, oxidative instability, or polymer breakdown. As polymer degradation progresses, the TP may experience reduced dispersion efficiency, leading to inconsistencies in activation temperature and decreased contrast between color states [79].

These findings highlight the progressive impact of mechanical recycling on thermochromic efficiency, reinforcing that higher pigment loading (PP92/TP8) accelerates optical deterioration, whereas pigment-free or lower-loaded blends (PP98/TP2) exhibit better thermochromic stability over multiple recycling cycles.

4. Conclusion

This study highlighted the feasibility of using TP in developing innovative smart food packaging. An evaluation of the effects of mechanical recycling on the optical and mechanical properties of polypropylene (PP) blends containing TP was undertaken. Significant information about the stability and functionality of food-grade thermochromic polymer blends in environmentally friendly food packaging applications was obtained by subjecting them to five recycling cycles.

The results showed that materials devoid of TP were the most recyclable, retaining their mechanical integrity with minimal changes to their thermal and optical characteristics. This blend was the best option for several recycling cycles, demonstrating the least deterioration in tensile strength, impact resistance, and thermochromic activation. In contrast, PP98/TP2 displayed moderate deterioration, with increased polymer brittleness and pigment clustering observed after three recycling cycles. The thermochromic response of this blend was still functional but showed a shift in activation temperature and reduced color vibrancy, suggesting limited recyclability for applications requiring precise thermochromic control.

The degradation was especially apparent in PP92/TP8, where high pigment concentrations greatly impacted mechanical stability, optical responsiveness, and thermal behavior. Severe pigment clustering and microcracking were found by SEM analysis, which resulted in the polymer matrix's embrittlement and decreased impact resistance.

A notable rise in activation temperature and apparent color fading rendered TP unsuitable for extended recyclability in food packaging applications.

Thermal analysis using differential scanning calorimetry (DSC) suggested that all TP blends exhibited progressive reductions in crystallinity, glass transition temperature (T_g), and melting enthalpy (H_m) with increasing recycling steps. However, the degradation rate correlated with TP concentration, reinforcing that TP influence the polymer's long-term recyclability. The temperature sensitivity of the blends changed with recycling cycles, where higher temperatures were required for complete thermochromic transitions, especially in PP92/TP8. This effect was attributed to polymer degradation, oxidation, and pigment agglomeration, which hindered the pigments' responsiveness to thermal stimuli.

Considering all factors, these results show how thermochromic functionality and recyclability are traded off in PP-based food packaging materials. Although TP benefit food safety and real-time temperature monitoring, their deterioration limits long-term use. Further research is required to consider stabilizing techniques, alternative pigment blends, or production adjustments to enhance the recyclability of thermochromic polymers in food packaging. These revelations support the continuous efforts to develop sustainable, intelligent packaging solutions that balance functionality, durability, and environmental responsibility.

 doi:10.20944/preprints202503.1564.v1

Author Contributions: Conceptualization, C.B.; methodology, C.B.; writing—original draft preparation, C.B.; writing—review and editing, C.B., D.M.C. and G.B.; supervision, J.G. and L.M.G.. All authors have read and agreed to the published version of the manuscript.

Funding: This research received no external funding.

Data Availability Statement: Not applicable.

Conflicts of Interest: The authors declare no conflicts of interest.

References

1. Jr, W.D.C.; Rethwisch, D.G. *Fundamentals of Materials Science and Engineering: An Integrated Approach*; John Wiley & Sons, 2020; ISBN 978-1-119-72367-7.
2. Shaji, J.S.; Paul, R.R. Smart Materials-Based E-Nose Technology: Fundamentals and Emerging Applications. In *New Advances in Materials Technologies*; Apple Academic Press, 2024 ISBN 978-1-003-45926-2.
3. Gillies, E.R. Reflections on the Evolution of Smart Polymers. *Israel Journal of Chemistry* **2020**, *60*, 75–85, doi:10.1002/ijch.201900075.
4. Bratek-Skicki, A. Towards a New Class of Stimuli-Responsive Polymer-Based Materials—Recent Advances and Challenges. *Applied Surface Science Advances* **2021**, *4*, 100068, doi:10.1016/j.apsadv.2021.100068.
5. Soo, X.Y.D.; Zhang, D.; Tan, S.Y.; Chong, Y.T.; Hui, H.K.; Sng, A.; Wei, F.; Suwardi, A.; Png, Z.M.; Zhu, Q.; et al. Ultra-High Performance Thermochromic Polymers via a Solid-Solid Phase Transition Mechanism and Their Applications. *Advanced Materials n/a*, 2405430, doi:10.1002/adma.202405430.
6. Hakami, A.; Srinivasan, S.S.; Biswas, P.K.; Krishnegowda, A.; Wallen, S.L.; Stefanakos, E.K. Review on Thermochromic Materials: Development, Characterization, and Applications. *J Coat Technol Res* **2022**, *19*, 377–402, doi:10.1007/s11998-021-00558-x.
7. Sadoh, A.; Hossain, S.; Ravindra, N.M. Thermochromic Polymeric Films for Applications in Active Intelligent Packaging—An Overview. *Micromachines* **2021**, *12*, 1193, doi:10.3390/mi12101193.
8. Cheng, Z.; Lei, L.; Zhao, B.; Zhu, Y.; Yu, T.; Yang, W.; Li, Y. High Performance Reversible Thermochromic Composite Films with Wide Thermochromic Range and Multiple Colors Based on Micro/Nanoencapsulated Phase Change Materials for Temperature Indicators. *Composites Science and Technology* **2023**, *240*, 110091, doi:10.1016/j.compscitech.2023.110091.
9. Dodero, A.; Escher, A.; Bertucci, S.; Castellano, M.; Lova, P. Intelligent Packaging for Real-Time Monitoring of Food-Quality: Current and Future Developments. *Applied Sciences* **2021**, *11*, 3532, doi:10.3390/app11083532.
10. Cheng, H.; Xu, H.; Julian McClements, D.; Chen, L.; Jiao, A.; Tian, Y.; Miao, M.; Jin, Z. Recent Advances in Intelligent Food Packaging Materials: Principles, Preparation and Applications. *Food Chemistry* **2022**, *375*, 131738, doi:10.1016/j.foodchem.2021.131738.
11. Yan, M.R.; Hsieh, S.; Ricacho, N. Innovative Food Packaging, Food Quality and Safety, and Consumer Perspectives. *Processes* **2022**, *10*, 747, doi:10.3390/pr10040747.
12. Roopa, H.; Panghal, A.; Kumari, A.; Chhikara, N.; Sehgal, E.; Rawat, K. Active Packaging in Food Industry. In *Novel Technologies in Food Science*; Chhikara, N., Panghal, A., Chaudhary, G., Eds.; Wiley, 2023; pp. 375–404 ISBN 978-1-119-77557-7.
13. George, J.; Kumar, R.; Aaliya, B.; Sunooj, K.V. Packaging Solutions for Monitoring Food Quality and Safety. In *Engineering Aspects of Food Quality and Safety*; Hebbar, H.U., Sharma, R., Chaurasiya, R.S., Ranjan, S., Raghavarao, K.S.M.S., Eds.; Springer International Publishing: Cham, 2023; pp. 411–442 ISBN 978-3-031-30683-9.
14. Wang, M.; Liu, G.; Gao, H.; Su, C.; Gao, J. Preparation and Performance of Reversible Thermochromic Phase Change Microcapsules Based on Negative Photochromic Spiropyran. *Colloids and Surfaces A: Physicochemical and Engineering Aspects* **2023**, *659*, 130808, doi:10.1016/j.colsurfa.2022.130808.
15. Civan, L.; Kurama, S. A Review: Preparation of Functionalised Materials/Smart Fabrics That Exhibit Thermochromic Behaviour. *Mater. Sci. Technolo.* **2021**, *37*, 1865–1877, doi:10.1080/02670836.2021.201584.

 doi:10.20944/preprints202503.1564.v1

16. Zhao, S.; Yuan, A.; Zhao, Y.; Liu, T.; Fu, X.; Jiang, L.; Lei, J. Preparation of Mechanically Robust and Thermochromic Phase Change Materials for Thermal Energy Storage and Temperature Indicator. *Energy and Buildings* **2022**, *261*, 111993, doi:10.1016/j.enbuild.2022.111993.
17. Hossain, S.; Sadoh, A.; Ravindra, N. Principles, Properties and Preparation of Thermochromic Materials. *Material Science & Engineering International Journal* **2023**, *7*, 146–156, doi:10.15406/mseij.2023.07.00218.
18. Cabello-Olmo, M.; Oneca, M.; Torre, P.; Díaz, J.; Encio, I.; Barajas, M.; Araña, M. Influence of Storage Temperature and Packaging on Bacteria and Yeast Viability in a Plant-Based Fermented Food. *Foods* **2020**, *9*, 302, doi:10.3390/foods9030302.
19. Grover, Y.; Negi, P.S. Recent Developments in Freezing of Fruits and Vegetables: Striving for Controlled Ice Nucleation and Crystallization with Enhanced Freezing Rates. *Journal of Food Science* **2023**, *88*, 4799–4826, doi:10.1111/1750-3841.16810.
20. Biegańska, M. Packaging of Dairy Products: Emerging Strategies. In *Food Packaging: The Smarter Way*; Shukla, A.K., Ed.; Springer Nature: Singapore, 2022; pp. 127–164 ISBN 978-981-16-7196-8.
21. Versino, F.; Ortega, F.; Monroy, Y.; Rivero, S.; López, O.V.; García, M.A. Sustainable and Bio-Based Food Packaging: A Review on Past and Current Design Innovations. *Foods* **2023**, *12*, 1057, doi:10.3390/foods12051057.
22. Mtibe, A.; Motloung, M.P.; Bandyopadhyay, J.; Ray, S.S. Synthetic Biopolymers and Their Composites: Advantages and Limitations—An Overview. *Macromolecular Rapid Communications* **2021**, *42*, 2100130, doi:10.1002/marc.202100130.
23. Adediji, Y.; Adediji, A. An Overview of Mechanical and Chemical Recycling Methods for Polyethylene Terephthalate Plastics 2024.
24. Prajapati, R.; Kohli, K.; Maity, S.K.; Sharma, B.K. Recovery and Recycling of Polymeric and Plastic Materials. In *Recent Developments in Plastic Recycling*; Parameswaranpillai, J., Mavinkere Rangappa, S., Gulihonnehalli Rajkumar, A., Siengchin, S., Eds.; Composites Science and Technology; Springer Singapore: Singapore, 2021; pp. 15–41 ISBN 978-981-16-3626-4.
25. Babaremu, K.; Adediji, A.; Olumba, N.; Okoya, S.; Akinlabi, E.; Oyinlola, M. Technological Advances in Mechanical Recycling Innovations and Corresponding Impacts on the Circular Economy of Plastics. *Environments* **2024**, *11*, 38, doi:10.3390/environments11030038.
26. *Sustainable Management of Urban Plastic Waste through Circular Economic Approaches*; Das, A.P., John, A., Eds.; First edition.; CRC Press: Boca Raton, FL, 2025; ISBN 978-1-003-46544-7.
27. Dey, A.; Dhumal, C.V.; Sengupta, P.; Kumar, A.; Pramanik, N.K.; Alam, T. Challenges and Possible Solutions to Mitigate the Problems of Single-Use Plastics Used for Packaging Food Items: A Review. *J Food Sci Technol* **2021**, *58*, 3251–3269, doi:10.1007/s13197-020-04885-6.
28. Ncube, L.K.; Ude, A.U.; Ogunmuyiwa, E.N.; Zulkifli, R.; Beas, I.N. Environmental Impact of Food Packaging Materials: A Review of Contemporary Development from Conventional Plastics to Polylactic Acid Based Materials. *Materials* **2020**, *13*, 4994, doi:10.3390/ma13214994.
29. Ncube, L.K.; Ude, A.U.; Ogunmuyiwa, E.N.; Zulkifli, R.; Beas, I.N. An Overview of Plastic Waste Generation and Management in Food Packaging Industries. *Recycling* **2021**, *6*, 12, doi:10.3390/recycling6010012.
30. Thushari, G.G.N.; Senevirathna, J.D.M. Plastic Pollution in the Marine Environment. *Heliyon* **2020**, *6*, e04709, doi:10.1016/j.heliyon.2020.e04709.
31. Mamun, A.A.; Prasetya, T.A.E.; Dewi, I.R.; Ahmad, M. Microplastics in Human Food Chains: Food Becoming a Threat to Health Safety. *Science of The Total Environment* **2023**, *858*, 159834, doi:10.1016/j.scitotenv.2022.159834.
32. Ibrahim, I.D.; Hamam, Y.; Sadiku, E.R.; Ndambuki, J.M.; Kupolati, W.K.; Jamiru, T.; Eze Agwo, A.; Snyman, J. Need for Sustainable Packaging: An Overview. *Polymers 14*, doi:10.3390/polym14204430.
33. ÇetiN, E.; Türkan, O.T. Material Recycling of Acrylonitrile Butadiene Styrene (ABS) from Wiring Devices Using Mechanical Recycling. *Sustainable Chemistry for the Environment* **2024**, *6*, 100095, doi:10.1016/j.scenv.2024.100095.

34. Khalid, M.Y.; Arif, Z.U.; Ahmed, W.; Arshad, H. Recent Trends in Recycling and Reusing Techniques of Different Plastic Polymers and Their Composite Materials. *Sustainable Materials and Technologies* **2022**, *31*, e00382, doi:10.1016/j.susmat.2021.e00382.
35. Mwanza, B.G. Introduction to Recycling. In *Recent Developments in Plastic Recycling*; Parameswaranpillai, J., Mavinkere Rangappa, S., Gulihonnehalli Rajkumar, A., Siengchin, S., Eds.; Composites Science and Technology; Springer Singapore: Singapore, 2021; pp. 1–13 ISBN 978-981-16-3626-4.
36. Luu, D.-N.; Barbaroux, M.; Dorez, G.; Mignot, K.; Doger, E.; Laurent, A.; Brossard, J.-M.; Maier, C.-J. Recycling of Post-Use Bioprocessing Plastic Containers—Mechanical Recycling Technical Feasibility. *Sustainability* **2022**, *14*, 15557, doi:10.3390/su142315557.
37. Vollmer, I.; Jenks, M.J.F.; Roelands, M.C.P.; White, R.J.; van Harmelen, T.; de Wild, P.; van der Laan, G.P.; Meirer, F.; Keurentjes, J.T.F.; Weckhuysen, B.M. Beyond Mechanical Recycling: Giving New Life to Plastic Waste. *Angewandte Chemie International Edition* **2020**, *59*, 15402–15423, doi:10.1002/anie.201915651.
38. Mulakkal, M.C.; Castillo Castillo, A.; Taylor, A.C.; Blackman, B.R.K.; Balint, D.S.; Pimenta, S.; Charalambides, M.N. Advancing Mechanical Recycling of Multilayer Plastics through Finite Element Modelling and Environmental Policy. *Resources, Conservation and Recycling* **2021**, *166*, 105371, doi:10.1016/j.resconrec.2020.105371.
39. Schyns, Z.O.G.; Shaver, M.P. Mechanical Recycling of Packaging Plastics: A Review. *Macromolecular Rapid Communications* **2021**, *42*, 2000415, doi:10.1002/marc.202000415.
40. Zou, L.; Xu, R.; Wang, H.; Wang, Z.; Sun, Y.; Li, M. Chemical Recycling of Polyolefins: A Closed-Loop Cycle of Waste to Olefins. *National Science Review* **2023**, *10*, nwad207, doi:10.1093/nsr/nwad207.
41. Zhao, X.; Copenhaver, K.; Wang, L.; Korey, M.; Gardner, D.J.; Li, K.; Lamm, M.E.; Kishore, V.; Bhagia, S.; Tajvidi, M.; et al. Recycling of Natural Fiber Composites: Challenges and Opportunities. *Resources, Conservation and Recycling* **2022**, *177*, 105962, doi:10.1016/j.resconrec.2021.105962.
42. Saikrishnan, S.; Jubinville, D.; Tzoganakis, C.; Mekonnen, T.H. Thermo-Mechanical Degradation of Polypropylene (PP) and Low-Density Polyethylene (LDPE) Blends Exposed to Simulated Recycling. *Polymer Degradation and Stability* **2020**, *182*, 109390, doi:10.1016/j.polymdegradstab.2020.109390.
43. de Camargo, R.V.; Saron, C. Mechanical–Chemical Recycling of Low-Density Polyethylene Waste with Polypropylene. *J Polym Environ* **2020**, *28*, 794–802, doi:10.1007/s10924-019-01642-5.
44. Satya, S.K.; Sreekanth, P.S.R. An Experimental Study on Recycled Polypropylene and High-Density Polyethylene and Evaluation of Their Mechanical Properties. *Materials Today: Proceedings* **2020**, *27*, 920–924, doi:10.1016/j.matpr.2020.01.259.
45. Shen, W.; Sui, S.; Yuan, W.; Wang, A.; Tao, Y.; Chen, S.; Deng, Z. Precise, Sensitive, and Reversible Thermochromic Luminescent Sensing Facilitated via Bright High-Temperature Luminescent $PEAMnBr_xI_{3-x}$ (x = 0/1/2/3). *J. Mater. Chem. C* **2021**, *9*, 2729–2737, doi:10.1039/D0TC05685E.
46. Supian, A.B.M.; Asyraf, M.R.M.; Syamsir, A.; Najeeb, M.I.; Alhayek, A.; Al-Dala'ien, R.N.; Manar, G.; Atiqah, A. Thermochromic Polymer Nanocomposites for the Heat Detection System: Recent Progress on Properties, Applications, and Challenges. *Polymers* **2024**, *16*, 1545, doi:10.3390/polym16111545.
47. Breheny, C.; Donlon, K.; Harrington, A.; Colbert, D.M.; Nunes Bezerra, G.S.; Geever, L. Thermochromic Polymers in Food Packaging: A Comprehensive Systematic Review and Patent Landscape Analysis. *Coatings* **2024**, *14*, 1252, doi:10.3390/coatings14101252.
48. Seeboth, A.; Lötzsch, D. *Thermochromic and Thermotropic Materials*; CRC Press, 2013; ISBN 978-981-4411-02-8.
49. Brighenti, R.; Li, Y.; Vernerey, F.J. Smart Polymers for Advanced Applications: A Mechanical Perspective Review. *Front. Mater.* **2020**, *7*, 196, doi:10.3389/fmats.2020.00196.
50. Chen, S.; Brahma, S.; Mackay, J.; Cao, C.; Aliakbarian, B. The Role of Smart Packaging System in Food Supply Chain. *Journal of Food Science* **2020**, *85*, 517–525, doi:10.1111/1750-3841.15046.
51. Shah, Y.A.; Bhatia, S.; Al-Harrasi, A.; Afzaal, M.; Saeed, F.; Anwer, M.K.; Khan, M.R.; Jawad, M.; Akram, N.; Faisal, Z. Mechanical Properties of Protein-Based Food Packaging Materials. *Polymers* **2023**, *15*, 1724, doi:10.3390/polym15071724.
52. Dorigato, A. Recycling of Polymer Blends. *Advanced Industrial and Engineering Polymer Research* **2021**, *4*, 53–69, doi:10.1016/j.aiepr.2021.02.005.

 doi:10.20944/preprints202503.1564.v1

53. Taş, M. Recycled PET-Based Thermochromic Nanofiber Membranes for Overheating Detection. *Opt Quant Electron* **2024**, *57*, 47, doi:10.1007/s11082-024-07977-1.
54. International Organization for Standardization ISO. *Plastics — Determination of Charpy Impact Properties — Part 1: Non-Instrumented Impact Test*; ISO 179-1; Geneva, Switzerland, **2023**.
55. International Organization for Standardization ISO. *Plastics — Determination of Tensile Properties — Part 2: Test Conditions for Moulding and Extrusion Plastics*; ISO 527-2; Geneva, Switzerland, **2012**.
56. College of Mechanical and Electrical Engineering, Beijing University of Chemical Technology, Beijing 100029, China; Fu, H.; Xu, H.; College of Mechanical and Electrical Engineering, Beijing University of Chemical Technology, Beijing 100029, China; Liu, Y.; State Key Laboratory of Organic-Inorganic Composites, Beijing University of Chemical Technology, Beijing, 100029, China; Yang, Z.; Department of Chemical and Biomolecular Engineering, The Ohio State University, Columbus, OH, USA; Department of Radiation Oncology, University of Texas Southwestern Medical Center, Dallas, TX, USA; Kormakov, S.; et al. Overview of Injection Molding Technology for Processing Polymers and Their Composites. *ES Mater.Manuf.* **2020**, doi:10.30919/esmm5f713.
57. International Organization for Standardization (ISO) International Organization for Standardization. *Plastics — Injection moulding of test specimens of thermoplastic materials — Part 1: General principles, and moulding of multipurpose and bar test specimens*; ISO 294-1; Geneva, Switzerland, **2017**.
58. Maris, J.; Bourdon, S.; Brossard, J.-M.; Cauret, L.; Fontaine, L.; Montembault, V. Mechanical Recycling: Compatibilization of Mixed Thermoplastic Wastes. *Polymer Degradation and Stability* **2018**, *147*, 245–266, doi:10.1016/j.polymdegradstab.2017.11.001.
59. Christodoulou, M.C.; Orellana Palacios, J.C.; Hesami, G.; Jafarzadeh, S.; Lorenzo, J.M.; Domínguez, R.; Moreno, A.; Hadidi, M. Spectrophotometric Methods for Measurement of Antioxidant Activity in Food and Pharmaceuticals. *Antioxidants* **2022**, *11*, 2213, doi:10.3390/antiox11112213.
60. Saunders, D. *Colour, Colour Measurement and Colour Change*; 1st ed.; Routledge: London, 2024; ISBN 978-1-003-39718-2.
61. Ren, X.; Zhang, Y.; Liu, Y.; Yang, C.; Dai, S.; Wang, X.; Liu, J. Preparation and Properties of Intrinsically Black Polyimide Films with CIE Lab Color Parameters Close to Zero and High Thermal Stability for Potential Applications in Flexible Printed Circuit Boards. *Polymers* **2022**, *14*, 3881, doi:10.3390/polym14183881.
62. ISO/CIE. *ISO/CIE 11664-4:2019—Colorimetry — Part 4: CIE 1976 Lab Colour Space**; ISO/CIE 11664-4; Geneva, Switzerland, **2019**.
63. Schröder, E.; Müller, G.; Arndt, K.-F. *Polymer Characterization*; Walter de Gruyter GmbH & Co KG, 2022; ISBN 978-3-11-247092-3.
64. Ceretti, D.V.A.; Edeleva, M.; Cardon, L.; D'hooge, D.R. Molecular Pathways for Polymer Degradation during Conventional Processing, Additive Manufacturing, and Mechanical Recycling. *Molecules* **2023**, *28*, 2344, doi:10.3390/molecules28052344.
65. Liu, Y.; Sharma, N. Selection of Property Methods and Estimation of Physical Properties for Polymer Process Modeling. In; 2023; pp. 41–86 ISBN 978-3-527-35267-8.
66. International Organization for Standardization ISO. *Plastics — Determination of the Melt Mass-Flow Rate (MFR) and Melt Volume-Flow Rate (MVR) of Thermoplastics — Part 1: Standard Method*; ISO 1133-1; Geneva, Switzerland, **2022**.
67. Lynch, J.M.; Corniuk, R.N.; Brignac, K.C.; Jung, M.R.; Sellona, K.; Marchiani, J.; Weatherford, W. Differential Scanning Calorimetry (DSC): An Important Tool for Polymer Identification and Characterization of Plastic Marine Debris. *Environmental Pollution* **2024**, *346*, 123607, doi:10.1016/j.envpol.2024.123607.
68. International Organization for Standardization ISO. *Plastics — Differential Scanning Calorimetry (DSC) — Part 3: Determination of Temperature and Enthalpy of Melting and Crystallization*; ISO 11357-3; Geneva, Switzerland, **2018**.
69. Lanyi, F.J.; Wenzke, N.; Kaschta, J.; Schubert, D.W. On the Determination of the Enthalpy of Fusion of α-Crystalline Isotactic Polypropylene Using Differential Scanning Calorimetry, X-Ray Diffraction, and

Fourier-Transform Infrared Spectroscopy: An Old Story Revisited. *Adv Eng Mater* **2020**, *22*, 1900796, doi:10.1002/adem.201900796.

70. Deshmukh, K.; Kovářík, T.; Muzaffar, A.; Basheer Ahamed, M.; Khadheer Pasha, S.K. Chapter 4—Mechanical Analysis of Polymers. In *Polymer Science and Innovative Applications*; AlMaadeed, M.A.A., Ponnamma, D., Carignano, M.A., Eds.; Elsevier, 2020; pp. 117–152 ISBN 978-0-12-816808-0.
71. Godzimirski, J.; Komorek, Z.; Komorek, A. An Energy Analysis of Impact Strength Tests Using Pendulum Hammers. *Adv. Sci. Technol. Res. J.* **2019**, *13*, 214–222, doi:10.12913/22998624/113051.
72. Zainuddin, H.; Ali, M.B.; Zakaria, K.A.; Paijan, L.H.; Mamat, M.F.; Abu Bakar, M.H. Investigation of Impact Properties under Instrumented Charpy Test. *J. Eng. Technol. Sci.* **2024**, *56*, 329–339, doi:10.5614/j.eng.technol.sci.2024.56.3.2.
73. Sharaf, S.; Santare, M.H.; Gerdes, J.; Advani, S.G. A Review of Factors That Influence the Fracture Toughness of Extrusion-Based Additively Manufactured Polymer and Polymer Composites. *Renew. Sustain. Energy Rev.* **2021**, *38*, doi:10.1016/j.rser.2020.101830.
74. Coceancigh, H.; Higgins, D.A.; Ito, T. Optical Microscopic Techniques for Synthetic Polymer Characterization. *Anal. Chem.* **2019**, *91*, 405–424, doi:10.1021/acs.analchem.8b04694.
75. Nechifor, M. Factors Influencing the Photochemical Behavior of Multicomponent Polymeric Materials. In *Photochemical Behavior of Multicomponent Polymeric-based Materials*; Rosu, D., Visakh P. M., Eds.; Advanced Structured Materials; Springer International Publishing: Cham, 2016; Vol. 26, pp. 21–65 ISBN 978-3-319-25194-3.
76. Sun, C.; Lux, S.; Müller, E.; Meffert, M.; Gerthsen, D. Versatile Application of a Modern Scanning Electron Microscope for Materials Characterization. *J Mater Sci* **2020**, *55*, 13824–13835, doi:10.1007/s10853-020-04970-3.
77. Solangi, N.H.; Karri, R.R.; Mubarak, N.M.; Mazari, S.A. Mechanism of Polymer Composite-Based Nanomaterial for Biomedical Applications. *Advanced Industrial and Engineering Polymer Research* **2024**, *7*, 1–19, doi:10.1016/j.aiepr.2023.09.002.
78. Maile, F.J. Colorants in Coatings. *Physical Sciences Reviews* **2021**, *6*, 707–789, doi:10.1515/psr-2020-0160.
79. Tatičková, Z.; Kudláček, J.; Zoubek, M.; Kuchař, J. Behaviour of Thermochromic Coatings under Thermal Exposure. *Coatings* **2023**, *13*, 642, doi:10.3390/coatings13030642.
80. Esmizadeh, E.; Tzoganakis, C.; Mekonnen, T.H. Degradation Behavior of Polypropylene during Reprocessing and Its Biocomposites: Thermal and Oxidative Degradation Kinetics. *Polymers (Basel)* **2020**, *12*, 1627, doi:10.3390/polym12081627.
81. Jiun, Y.L.; Tze, C.T.; Moosa, U.; Tawawneh, M.A. Effects of Recycling Cycle on Used Thermoplastic Polymer and Thermoplastic Elastomer Polymer. *Polymers and Polymer Composites* **2016**, *24*, 735–740, doi:10.1177/096739111602400909.
82. Oblak, P.; Gonzalez-Gutierrez, J.; Zupančič, B.; Aulova, A.; Emri, I. Processability and Mechanical Properties of Extensively Recycled High Density Polyethylene. *Polymer Degradation and Stability* **2015**, *114*, 133–145, doi:10.1016/j.polymdegradstab.2015.01.012.
83. Athulya Wickramasingha, Y.; Dharmasiri, B.; Randall, J.D.; Yin, Y.; Andersson, G.G.; Nepal, D.; Newman, B.; Stojcevski, F.; Eyckens, D.J.; Henderson, L.C. Surface Modification of Carbon Fiber as a Protective Strategy against Thermal Degradation. *Composites Part A: Applied Science and Manufacturing* **2022**, *153*, 106740, doi:10.1016/j.compositesa.2021.106740.
84. Pielichowski, K.; Njuguna, J.; Majka, T.M. *Thermal Degradation of Polymeric Materials*; Elsevier, 2022; ISBN 978-0-12-823142-5.
85. Yousif, E.; Ahmed, D.; Zainulabdeen, K.; Jawad, A. Photo-Physical and Morphological Study of Polymers: A Review. *Phys. Chem. Res. 11*, 409–424, doi:10.22036/pcr.2022.342751.2105.
86. Patel, A.D.; Schyns, Z.O.G.; Franklin, T.W.; Shaver, M.P. Defining Quality by Quantifying Degradation in the Mechanical Recycling of Polyethylene. *Nat Commun* **2024**, *15*, 8733, doi:10.1038/s41467-024-52856-8.
87. Lamtai, A.; Elkoun, S.; Robert, M.; Mighri, F.; Diez, C. Mechanical Recycling of Thermoplastics: A Review of Key Issues. *Waste* **2023**, *1*, 860–883, doi:10.3390/waste1040050.
88. Titone, V.; Botta, L.; La Mantia, F.P. Mechanical Recycling of New and Challenging Polymer Systems: A Brief Overview. *Macro Materials & Eng* **2025**, *310*, 2400275, doi:10.1002/mame.202400275.

89. Cecon, V.S.; Pham, T.; Curtzwiler, G.; Vorst, K. Assessment of Different Application Grades of Post-Consumer Recycled (PCR) Polyolefins from Material Recovery Facilities (MRFs) in the United States. *ACS Appl. Polym. Mater.* **2024**, *6*, 13065–13076, doi:10.1021/acsapm.4c01927.
90. Pfaendner, R. Restabilization—30 Years of Research for Quality Improvement of Recycled Plastics Review. *Polymer Degradation and Stability* **2022**, *203*, 110082, doi:10.1016/j.polymdegradstab.2022.110082.
91. Dintcheva, N.T. Overview of Polymers and Biopolymers Degradation and Stabilization towards Sustainability and Materials Circularity. *Polymer* **2024**, *306*, 127136, doi:10.1016/j.polymer.2024.127136.
92. Liedl, B.; Höftberger, T.; Burgstaller, C. Properties of Multiple-Processed Natural Short Fiber Polypropylene and Polylactic Acid Composites: A Comparison. *Macromol* **2024**, *4*, 723–738, doi:10.3390/macromol4040043.
93. Nagare, S.M.; Hakami, A.; Biswas, P.K.; Stefanakos, E.K.; Srinivasan, S.S. A Review of Thermochromic Materials for Coating Applications: Production, Protection, and Degradation of Organic Thermochromic Materials. *J Coat Technol Res* **2025**, *22*, 91–115, doi:10.1007/s11998-024-00982-9.
94. El-Mohtadi, F.; d'Arcy, R.; Tirelli, N. Oxidation-Responsive Materials: Biological Rationale, State of the Art, Multiple Responsiveness, and Open Issues. *Macromol. Rapid Commun.* **2019**, *40*, 1800699, doi:10.1002/marc.201800699.
95. Shojaeiarani, J.; Bajwa, D.S.; Rehovsky, C.; Bajwa, S.G.; Vahidi, G. Deterioration in the Physico-Mechanical and Thermal Properties of Biopolymers Due to Reprocessing. *Polymers* **2019**, *11*, 58, doi:10.3390/polym11010058.
96. Loaeza, D.; Cailloux, J.; Santana Pérez, O.; Sánchez-Soto, M.; Maspoch, M. Impact of Titanium Dioxide in the Mechanical Recycling of Post-Consumer Polyethylene Terephthalate Bottle Waste: Tensile and Fracture Behavior. *Polymers* **2021**, *13*, 310, doi:10.3390/polym13020310.
97. Lan, T.; Qian, S.; Song, T.; Zhang, H.; Liu, J. The Chromogenic Mechanism of Natural Pigments and the Methods and Techniques to Improve Their Stability: A Systematic Review. *Food Chemistry* **2023**, *407*, 134875, doi:10.1016/j.foodchem.2022.134875.
98. Billingham, N.; Knight, B.; Garside, P.; Mills, D. Polymers and Their Degradation. In *Conservation of Books*; Routledge: London, 2023; pp. 385–416 ISBN 978-1-003-16267-4.
99. *Bioinspired Inorganic Materials: Structure and Function*; Hall, S.R., Ed.; Inorganic Materials Series; Royal Society of Chemistry: Cambridge, 2019; ISBN 978-1-78801-146-4.
100. Zhu, P.; Zhou, C.; Wang, Y.; Sauer, B.; Hu, W.; Dong, X.; Wang, D. Reversible–Irreversible Transition of Strain-Induced Crystallization in Segmented Copolymers: The Critical Strain and Chain Conformation. *ACS Appl. Polym. Mater.* **2021**, *3*, 3576–3585, doi:10.1021/acsapm.1c00462.
101. Wei, Z.; Gerke, S.; Brünig, M. Ductile Damage and Fracture Characterizations in Bi-Cyclic Biaxial Experiments. *International Journal of Mechanical Sciences* **2024**, *276*, 109380, doi:10.1016/j.ijmecsci.2024.109380.
102. Allen, N.S.; Edge, M. Perspectives on Additives for Polymers. 1. Aspects of Stabilization. *Vinyl Additive Technology* **2021**, *27*, 5–27, doi:10.1002/vnl.21807.
103. Randhawa, K.S. Polymer Composites with Advanced Pigments: Enhancing Properties and Applications. *PRT* **2024**, doi:10.1108/PRT-02-2024-0019.
104. Randhawa, K.S. Synthesis, Properties, and Environmental Impact of Hybrid Pigments. *The Scientific World Journal* **2024**, *2024*, 2773950, doi:10.1155/tswj/2773950.
105. Dungani, R.; Sumardi, I.; Alamsyah, E.M.; Aditiawati, P.; Karliati, T.; Malik, J.; Sulistyono A Study on Fracture Toughness of Nano-Structured Carbon Black-Filled Epoxy Composites. *Polym. Bull.* **2021**, *78*, 6867–6885, doi:10.1007/s00289-020-03444-5.